Report DREO (Geophysics) 33

ANALYSIS AND PREDICTION OF GROUSER THRUST ON SAND

R.N. Yong and R. Sylvestre-Williams

Soil Mechanics Series - No. 26

November, 1969

SOIL MECHANICS LABORATORY

McGILL UNIVERSITY

DEPARTMENT OF CIVIL ENGINEERING AND APPLIED MECHANICS

MONTREAL, CANADA

REPORT TO
DEFENCE RESEARCH ESTABLISHMENT, OTTAWA
DEFENCE RESEARCH BOARD, CANADA

DEPARTMENT OF DEFENCE PRODUCTION, CONTRACT
NO. GR. 813009
SERIAL NO. 2GR8-21

ANALYSIS AND PREDICTION OF GROUSER THRUST ON SAND

by

R.N. Yong and R. Sylvestre-Williams
Soil Mechanics Laboratory

Department of Civil Engineering
and Applied Mechanics

McGill University
Montreal, Quebec.

Report for

Defence Research Establishment Ottawa
Defence Research Board
Ottawa, Ontario.

D.D.P. Contract No. GR.813009, Serial No. 2GR8-21

November 1969

PREFACE

In the following report on the problem of grouser-soil interaction, we direct our attention to a study of the mechanics of grouser motion on sand. The aim of the study is to provide not only an analysis of the mechanics of interaction, but also to provide (through the analysis) a means for predicting the developed thrust (or force) due to the aggressive action of the grouser.

It is shown that the limit equilibrium approach can be used successfully to arrive at theoretically computed thrust values which compare very well with measured values. In addition, the shape and size of failure surfaces under the grouser can be predicted using the method of characteristics. In Chapter 1, the overall perspective provides a capsule idea of the intent and results of the study. It is shown that general application of the theory can be sought for the particular case at hand.

This study on grouser-soil interaction was conducted as part of the overall soil-vehicle interaction study, under contract arrangement with the Defence Research Establishment, Ottawa (DREO), Geophysics Section, negotiated through the Department of Defence Production. Acknowledgement is made to Mr. T.A. Harwood, Chief, Geophysics Section, DREO, project officer for this study.

Dr. R.D. Japp provided general assistance in the conduct of the study. C.K. Chen assisted in machine computation.

CHAPTER 1

OVERALL PERSPECTIVE

1.1 INTRODUCTION

In the previous reports concerned with wheel-clay interaction*, it has been shown that energy losses resulting from interfacial slip and subsoil deformation can be computed from an examination of the soil deformation at the wheel-soil interface and at some depth to provide for an almost exact prediction of the drawbar pull from a known torque input value. Whilst the previous studies have been concerned with the problem of rigid wheel motion on clay soils, the lessons learned from observation of soil deformation under the moving wheel demonstrate the fact that similar techniques should be used to define and evaluate the mechanics of grouser-soil interaction.

Thus in view of the fact that the locomotive ability of any vehicle is dependent on its interaction with soil, it becomes obvious that in describing, for example, the performance of a tracked vehicle on soil, a better understanding of the mechanics of the interaction between grouser and soil will provide for a more rational basis for evaluation of vehicle performance. Previous attempts at examining the geometry of the failure surface beneath a moving rigid grouser have been reported (e.g., Bekker

---

* "Drawbar Pull Prediction from Energy Losses in Wheel-Clay Interaction" by Yong and Fitzpatrick-Nash, Soil Mechanics Series No. 22, Report DRTE (Geophysics) 29, August 1968.

"Response Behaviour of Clay Soil Under a Moving Rigid Wheel" by Yong, Fitzpatrick-Nash and Webb, Soil Mechanics Series No. 23, Report DRTE (Geophysics) 30, September 1968.

"Energy Considerations in Wheel-Clay Soil Interaction" by Yong and Webb, Soil Mechanics Series No. 25, Report DREO (Geophysics) 32.

1960; Haythornthwaite, 1961). Apparently, investigations into the mode and mechanism of failure appear to be quite limited. Except for the latter work it would appear that the emphasis on research into this problem has centered around the use of the strip footing model. Modifications introduced through further research have been directed towards improving the constraints and providing for a better definition of the boundary conditions.

1.2 THE PROBLEMS STUDIED IN THIS REPORT

In this report we are concerned with the mechanics of a single grouser acting on sand as a first phase of the study of grouser-soil interaction. The experimental problem is reduced to a plane strain condition where a glass-sided box is used to provide for grid markings to assist in visual observation of soil deformation under the action of the grouser. The intent here is to provide information on the physical behaviour of a single grouser in order to formulate the necessary mathematical model and boundary conditions.

From initial observations of the generated failure surface, it became apparent that the limit equilibrium approach could be utilized, and thus further experimental observations were directed towards defining the limits of applicability of the solution technique and also the extent of the failed soil mass under the aggressive action of the moving grouser. The method of characteristics has been used as an additional means for solution of the problem in order to provide for a comparison between the predicted failure characteristics and the actual slip line observed from experimentation.

The use of sand as an initial examination of the problem provides for a limiting case for study in the hope that the method of analysis generated could be modified for application to other soil types. In this, the study of the mechanics of grouser-soil interaction, the use of the limit equilibrium method of analysis provides for a tool for prediction or analytical computation of the horizontal and vertical forces necessary to provide for aggressive action of the grouser. We define aggressive grouser action to mean motion of the grouser into the soil to create a failure condition in the soil. Thus the limits of the magnitudes of the horizontal and vertical forces defined for aggressive action of the grouser serve to identify the maximum forces that can be applied to provide for forward motion of the tracked vehicle.

In the application of the rigorous method of characteristics, the failure characteristic if identified as corresponding to the actual sub-surface observed experimentally, would provide justification for the limit equilibrium approach of study to the problem. It will be shown in this particular report that such is the case and it therefore appears that for a cohesionless material, the limit equilibrium technique and method of characteristics solutions can be applied to analyze the problem and provide for a tool for predicting the forward motion of a tracked vehicle.

1.3 EXPERIMENTAL CONSIDERATIONS

The grouser tests performed in this study fall into two categories, viz:

1. Constant Vertical Load Tests (CVL), and
2. Constant Elevation (CE) Tests.

1. Constant Vertical Load Tests

   A constant vertical load intended to simulate a portion of the vehicle weight was applied to the top of the grouser and maintained throughout the entire test. Since the grouser was mounted on a carriage, it was free to translate both vertically and horizontally but was restrained against rotation. The measurable response parameters during this type of test were the horizontal displacement, the horizontal force and the vertical displacement. Since all of these measurements were taken at the same time with a common time base, the velocity of horizontal translation was also determined.

2. Constant Elevation Tests

   In this particular series, the grouser was restrained in a vertical direction and was only free to translate horizontally. The method of restraint kept the grouser at a constant height in relation to the initial sand surface throughout the duration of the test.

   As a result of the vertical restraint, the measurable response parameters in this type of test were once more the horizontal force and horizontal displacement and hence velocity. However, instead of a vertical displacement, the force required to restrain the grouser vertically was measured.

It was reasoned that these two types of tests would simulate most situations which arise in practice and the results obtained therefrom should be representative of the behaviour of the soil mass under the most common loading systems which can be applied to a grouser.

In each of the two principal types of tests, any one of several variables may be considered. Since the response of the soil to a given forcing function is sensitive to each of these variables, it became necessary to select those variables which, it was estimated, would be the most important for this first phase of grouser study. To this end the following test variables were selected:

1. Grouser Geometry - i.e., the variation of the ratio h/ℓ as defined in Figure 1-1. The value of ℓ was kept constant at 3 inches and differences in the h/ℓ ratio were achieved by changing h.

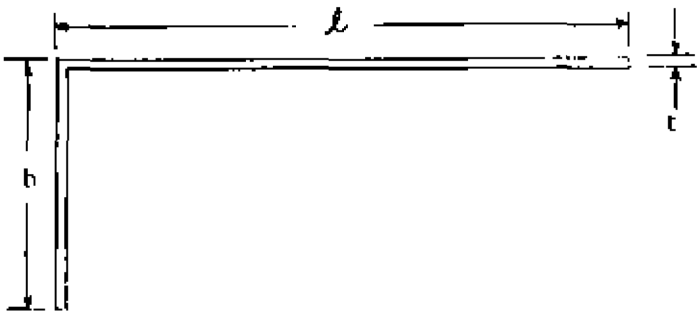

FIGURE 1-1. GROUSER GEOMETRY

2. System Variables
    a) Horizontal Velocity
    b) Initial Vertical Load.

1.3.1 Apparatus

The test apparatus consisted of a grouser plate rigidly attached to a carriage which allowed it to translate both horizontally and vertically but which permitted no angular rotation (see Figure 1.2).

The carriage itself was mounted on roller bearings which travelled in polished guide rails. The rails were machined to a tolerance of 0.003 inches, and as a consequence the frictional resistance of the system was reduced to a minimum, the force required to overcome this resistance being typically of the order of 2% to 4% of the total measured horizontal force.

The carriage, with the attached grouser, was driven at a constant velocity by means of a hydraulically powered piston. The hydraulic system was so constructed that the fluid pressure applied to the piston was, for all practical purposes, constant in time and as such, the velocity of the piston, once the initial acceleration had reduced to zero, was constant.

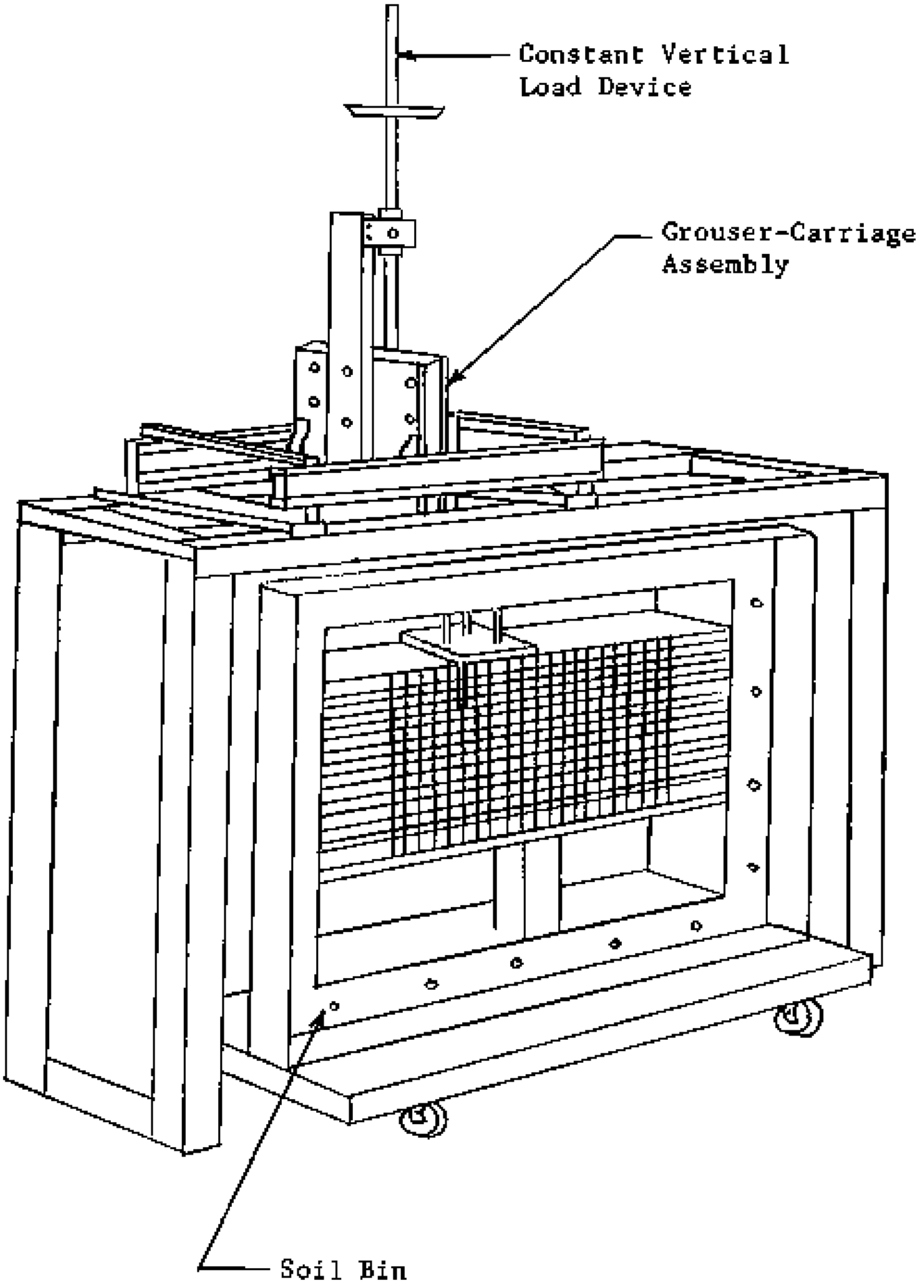

FIGURE 1-2. ISOMETRIC VIEW OF EXPERIMENTAL APPARATUS

By varying the fluid pressure applied to the piston and by adjusting the rate of discharge of the fluid, the piston speed was continuously variable between the limits of 1 inch per second and 25 inches per second.

To ensure that the piston velocity was at its maximum value at the beginning of the test, the 12 inch stroke capacity piston was allowed to travel for a distance of approximately 4 inches before contacting the grouser carriage. In view of the fact that the rise time of the velocity to its maximum value was generally of the order of 0.5 seconds at the lowest speeds tested, this distance was sufficient for the piston to build up to full speed.

The carriage and grouser assembly were mounted on a frame in such a position that it was directly above a soil bin whose dimensions were 22-1/2 inches x 4 inches in planform and which usually accommodated a depth of sand of the order of 9 inches. The bin was equipped with removable lucite side walls and was mounted on castors to facilitate its removal from under the carriage. The carriage and bin are shown in Figure 1-2.

1.3.2 Measuring and Recording Devices

All force and displacement measurements were made by means of electrical transducers. For measurement of sand deformation and assessment of sand performance during the aggressive action of the grouser, a black sand marker grid was superposed on the surface side of the sand in the container. A 16 mm cine camera was used to record continuous grid distortion during the tests.

1.4 SUMMARY AND OUTLOOK

From the test results, it appears that the method of solution shown in Chapters 2 and 3 provides a viable means for predicting and analyzing grouser-soil interaction. For convenience, we can summarize three key graphs to show (schematically) the success achieved in correlation between theoretically predicted (or computed) and actual measured values (see Figure 1.3). The actual graphs may be seen in Chapter 3 where the proper discussion is provided accordingly.

Having established the viability of the method, and its superiority to present reported methods - as evident from Figure 1-3 and Chapter 3, it would appear that further study on multiple grousers is in order. The end purpose of multiple grouser study is to determine optimum spacing to achieve best total aggressive grouser motion. This would lead to a more rational basis for design of grouser spacing.

In actual fact, it will be seen that grouser spacing can be established from a single grouser test - in view of the success achieved in correlation between theory applied here and actual experimentation. Attention is directed towards the analytical model shown in Figure 2-2 and the fact that this formed the basis for the theoretical considerations. Thus by placing the next grouser beyond the Rankine zone shown in Figure 2-2, taking into account the dependence of α and β on grouser and system parameters, a rational set of rules may be devised to aid in studying grouser spacing. This outlook is further discussed in the latter part of this report.

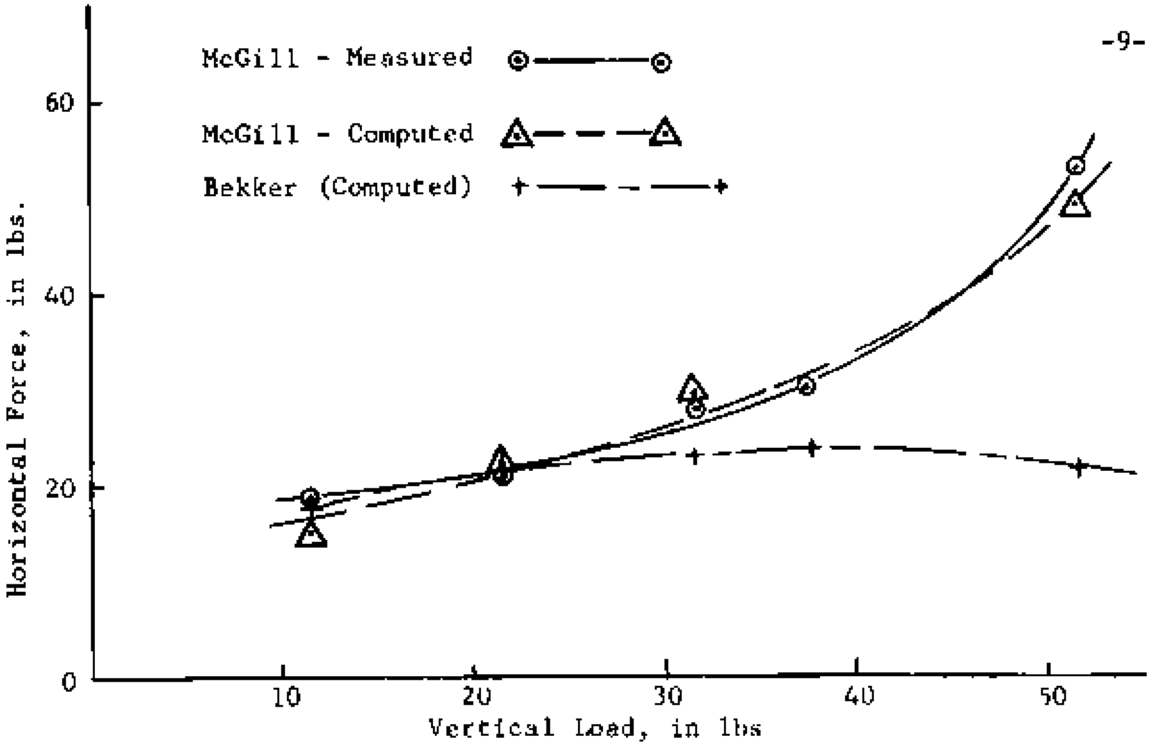

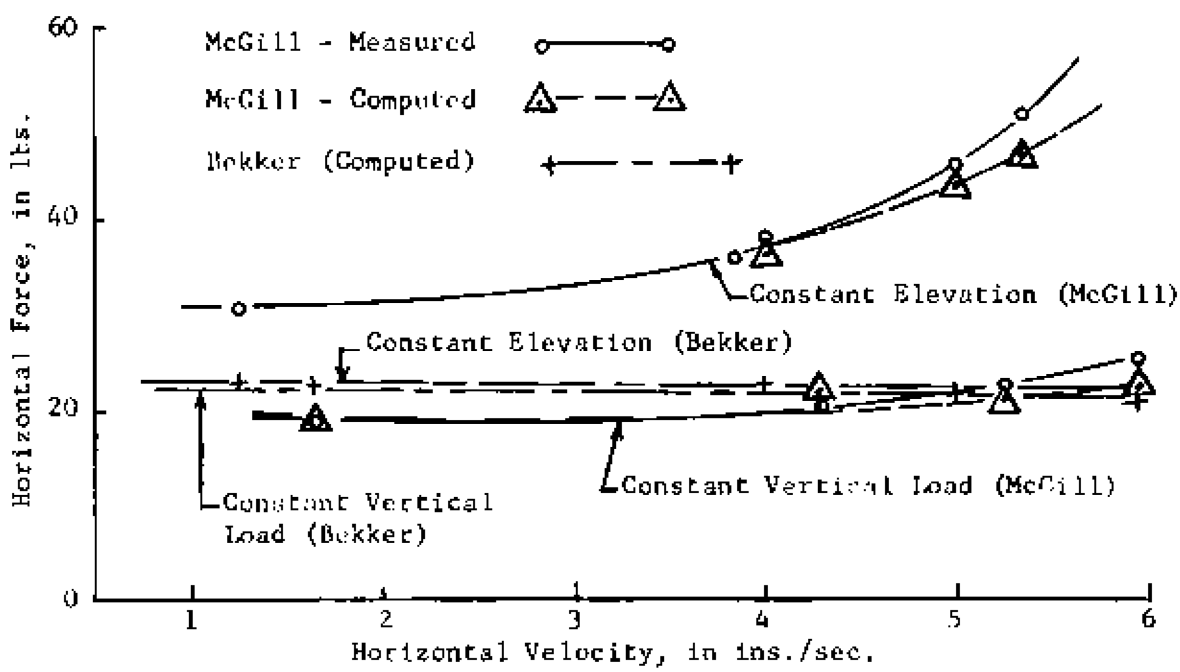

FIGURE 1-3. COMPARISON OF EXPERIMENTALLY MEASURED AND COMPUTED HORIZONTAL FORCES AS FUNCTIONS OF APPLIED LOAD AND CARRIAGE VELOCITY

CHAPTER 2

THEORETICAL CONSIDERATIONS

2.1 INTRODUCTION

From initial tests with the grouser, using a gridded glass-sided box, the geometry of the failure mass under the aggressive action of the grouser showed patterns similar to that shown in Figure 2-1. With this knowledge of the physical behaviour of the soil mass, a theoretical solution can now be sought.

2.2 ANALYTICAL MODEL

The analytical model shown in Figure 2-2 may be constructed from Figure 2-1. We note that the deforming soil mass is broken down into three parts, namely:

a) rigid zone where the soil in this region may be assumed to be an integral part of the grouser. At a later time, it will be shown that the boundaries of this rigid zone are dependent on both grouser geometry and constraints surrounding the aggressive movement of the grouser, i.e., β and α are influenced by the foregoing factors.

b) a zone of radial shear, and

c) a Rankine passive zone.

It is apparent that a theoretical solution may be sought in terms of limit equilibrium if reasonable assurance is provided by the knowledge that all the material in the radial and passive zones are at the limiting state of equilibrium. Whilst in actual fact this is a difficult condition to meet, some departure from this rigid requirement may be tolerated in actual practice.

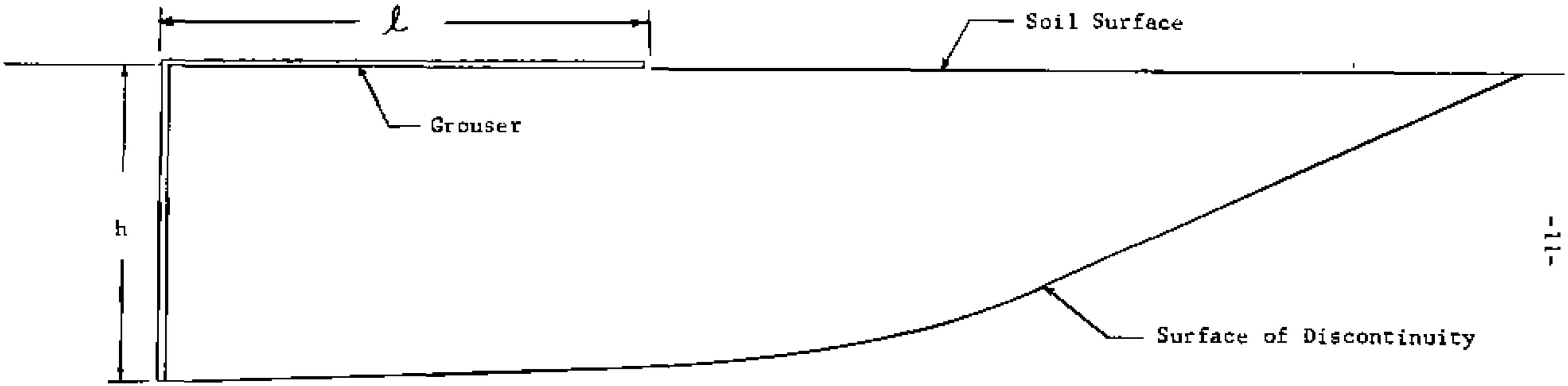

FIGURE 2-1. GEOMETRY OF PLASTIC REGION BENEATH GROUSER PLATE

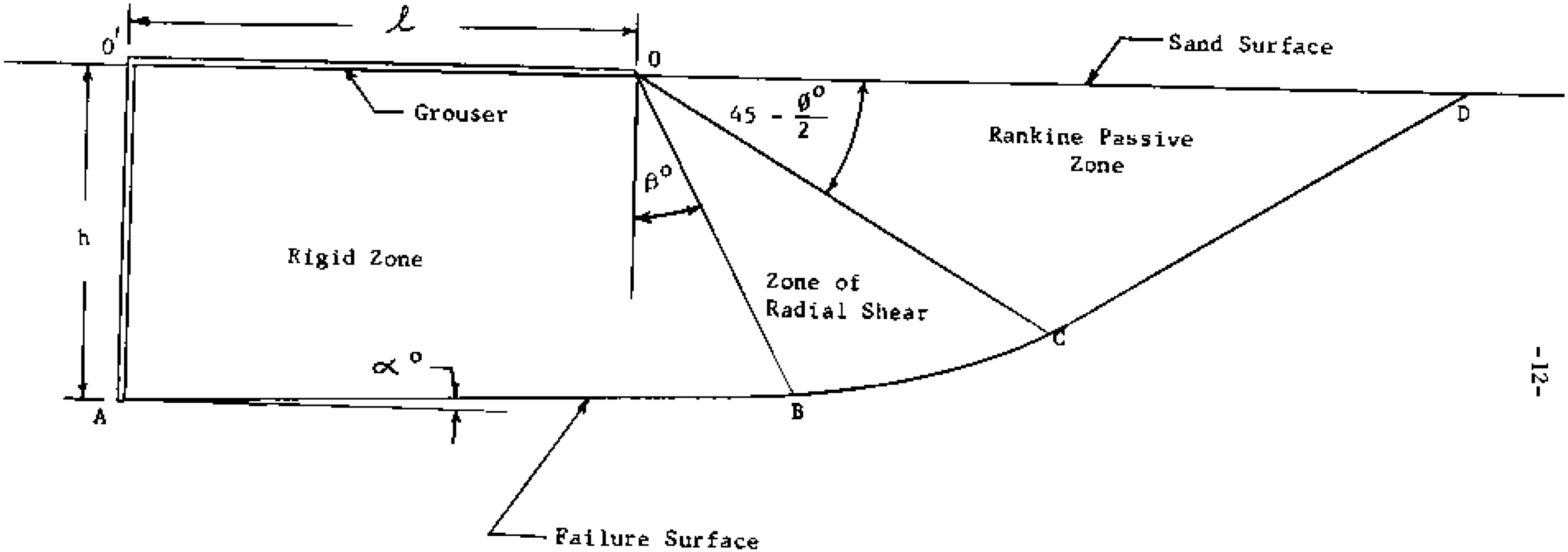

FIGURE 2-2. GEOMETRY OF FAILURE ZONE BENEATH GROUSER PLATE

Accepting the constraints imposed from physical behaviour and with some reasonable assurance that the material in the radial and passive zones is in a failable state, the following sections will be devoted to providing the limit equilibrium solution for the model shown in Figure 2-2.

2.3 THE METHOD OF LIMIT EQUILIBRIUM

In this section, the equations necessary for the solution of the grouser problem under study, using the techniques of limit equilibrium, will be developed, together with the boundary conditions necessary for the solution of these differential equations. The equations describing the geometry of the failure surface using the method of characteristics will also be developed.

Referring to Figure 2-2, if we assume that the surface of discontinuity (i.e., line OB) represents a rigid surface, then the method as developed by Yong et al, 1969, may be applied to obtain a stress distribution in the radial and passive zones. Whilst there may be no rigorous theoretical justification for such an assumption, experimental evidence obtained suggests the validity of this assumption.

One of the principal consequences of the assumption that OB represents a rigid surface is the requirement that zone OBCDO moves upwards, or downwards, in relation to zone O'ABO. From an examination of the displacement patterns of the grid nodes and of the velocity fields (shown in a later section of this report) it was noted that the velocity in this region was essentially zero, relative to the grouser plate. As such, it was concluded that zone OBCDO moved upward, or downward, in relation to zone O'ABO.

With this assumption, the method of limit equilibrium may then be used to provide a simplified solution to the field equations, provided that the following additional assumptions are made:

1. that the failure configuration, shown in Figure 2-3, consists of three zones. Zone OCD may be treated as a Rankine Passive zone, with the major principal stress direction being horizontal, while zone OBC consists of a transition zone, where the material is in a state of radial shear and zone O'ABO is a simplified rigid zone. This is not unlike the assumptions made in the classical bearing capacity problems developed by Terzaghi (1944).
2. that all of the material within the failure zone is in a state of limit stability or at impending shear failure.
3. that the material is homogeneous, isotropic and incompressible, and
4. that the value of the term $\frac{\rho u^2}{\sigma} \ll 1$. Thus the inertia terms of the form $v_x \frac{\partial(\rho v_x)}{\partial x}$ may be neglected. It follows that the equations of equilibrium, rather than the equations of momentum, may be used to describe the state of stress within the material.

With these assumptions, a solution may then be found for the following system of equations.

2.3.1 Equations of Equilibrium

The differential equations of equilibrium in polar coordinate form (consistent with the coordinates shown in Figure 2-3) are given as follows:

$$\frac{\partial \sigma_r}{\partial r} + \frac{1}{r}\frac{\partial \tau_{r\theta}}{\partial \theta} + \frac{\sigma_r - \sigma_\theta}{r} = \rho g \cos\theta \tag{2.1}$$

$$\frac{\partial \tau_{r\theta}}{\partial r} + \frac{1}{r}\frac{\partial \sigma_\theta}{\partial \theta} + 2\frac{\tau_{r\theta}}{r} = -\rho g \sin\theta$$

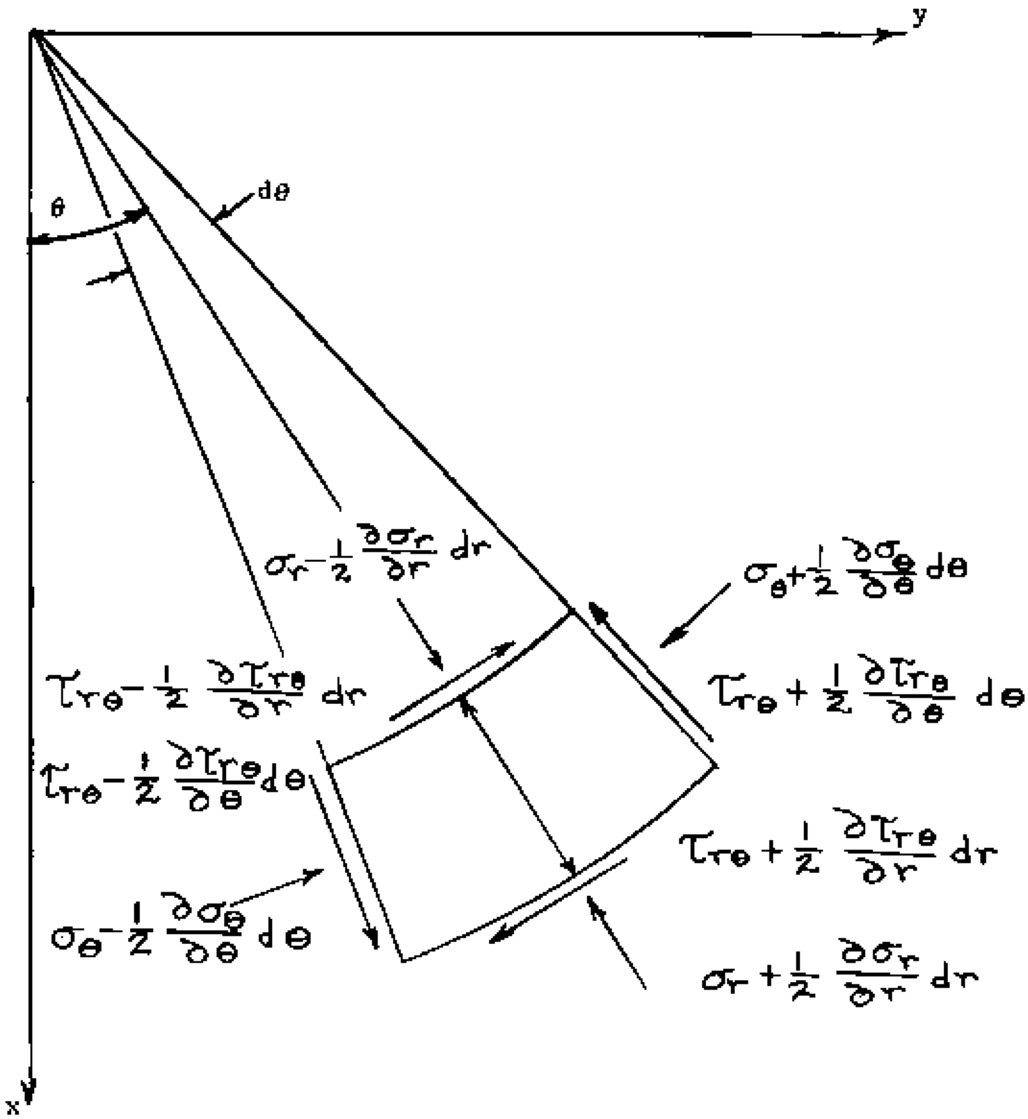

FIGURE 2-3. STRESS NOTATION CONVENTION IN POLAR COORDINATE SYSTEM

2.3.2 Yield Criterion

The Mohr-Coulomb failure criterion, valid for the description of the stress state in a granular material at the point of impending failure, may be expressed as:

$$\sigma_x = \frac{\sigma_x+\sigma_y}{2}(1 + \sin\phi \cos 2\psi)$$

$$\sigma_y = \frac{\sigma_x+\sigma_y}{2}(1 - \sin\phi \cos 2\psi) \qquad (2.2)$$

$$\tau_{xy} = \frac{\sigma_x+\sigma_y}{2} \sin\phi \sin 2\psi$$

where: ψ = angle of inclination of major principal stress to the x-axis.

Denoting the inclination of the major principal stress direction to the θ-axis as ψ', equations (2.2) can be written, in terms of $r - \theta$ coordinates, as:

$$\sigma_r = \frac{\sigma_r+\sigma_\theta}{2}(1 + \sin\phi \cos 2\psi')$$

$$\sigma_\theta = \frac{\sigma_r+\sigma_\theta}{2}(1 - \sin\phi \cos 2\psi') \qquad (2.3)$$

$$\tau_{r\theta} = \frac{\sigma_r+\sigma_\theta}{2} \sin\phi \sin 2\psi'$$

The geometry of the principal stresses in the physical plane is shown in Figure 2-5.

For the general case of a rigid surface moving through a soil, the stresses acting on the rigid surface may be expressed as:

$$\tau_{r\theta} = \sigma_\theta \tan\delta \quad \text{in the passive case, and}$$
$$\tau_{r\theta} = -\sigma_\theta \tan\delta \quad \text{in the active case} \qquad (2.4)$$

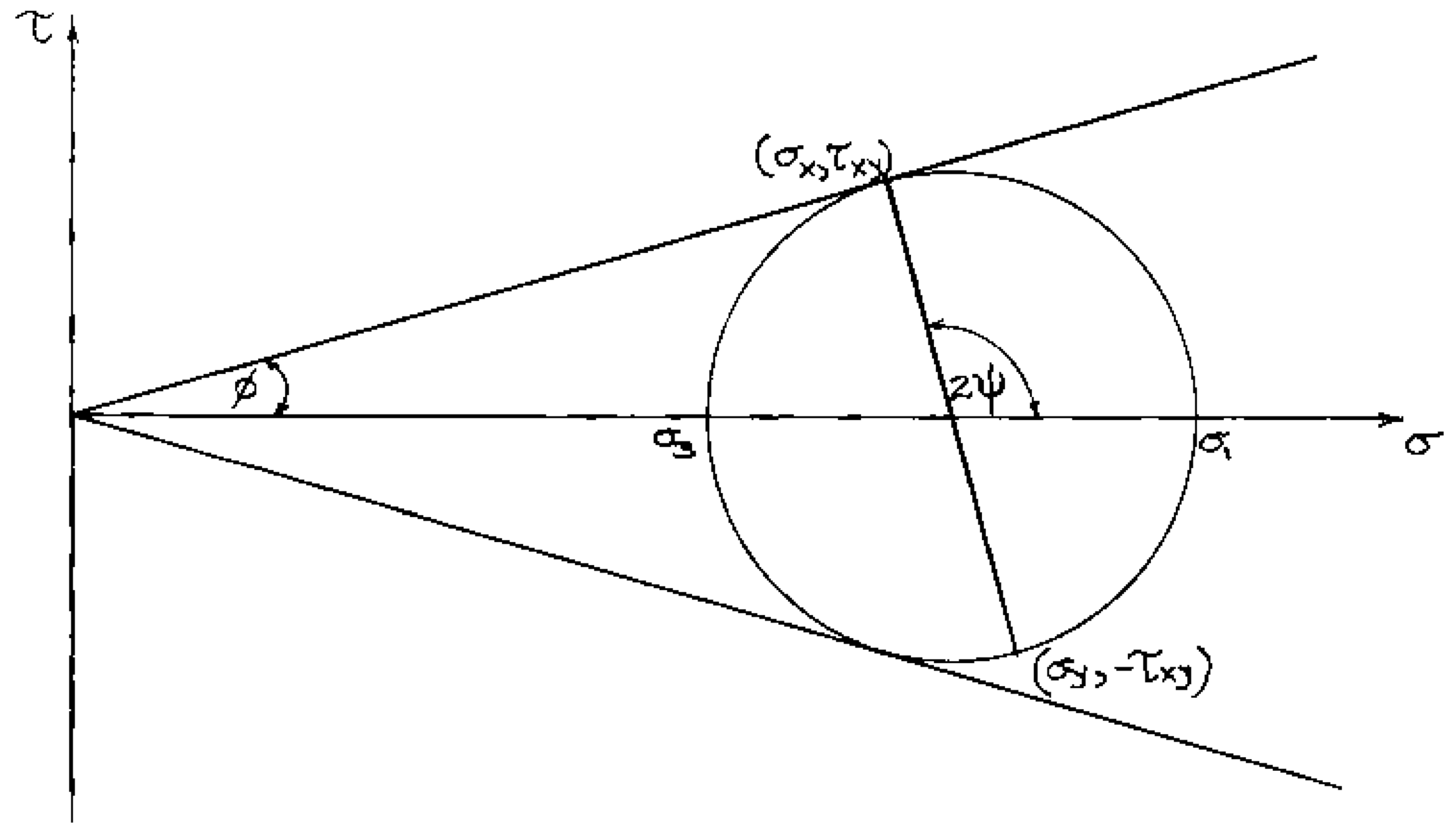

FIGURE 2-4. MOHR-COULOMB REPRESENTATION FOR A FRICTIONAL (C = 0) MATERIAL

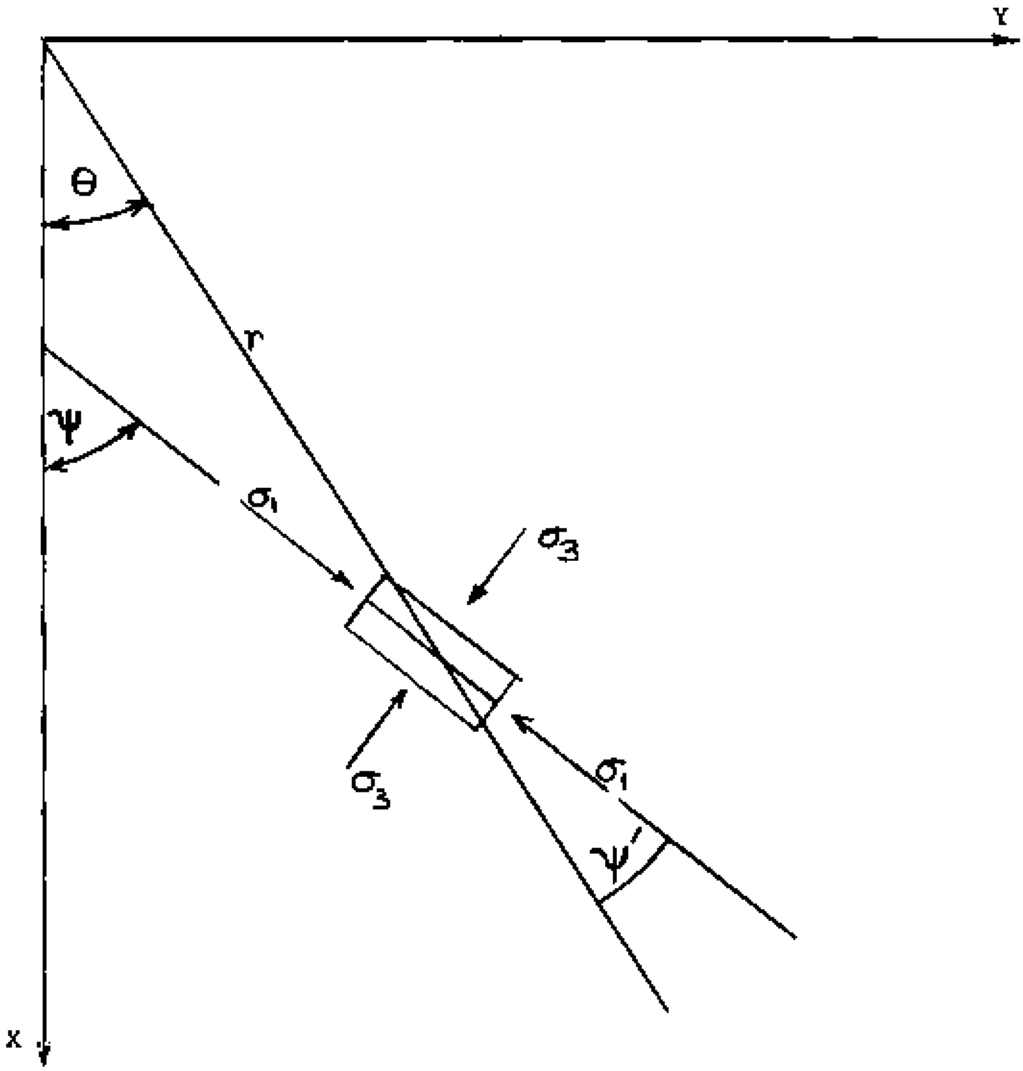

FIGURE 2-5. PRINCIPAL STRESS REPRESENTATION IN THE PHYSICAL PLANE

where: δ = angle of friction between the surface and the soil.

The geometry of the forces acting on the surface may be seen in Figure 2-6.

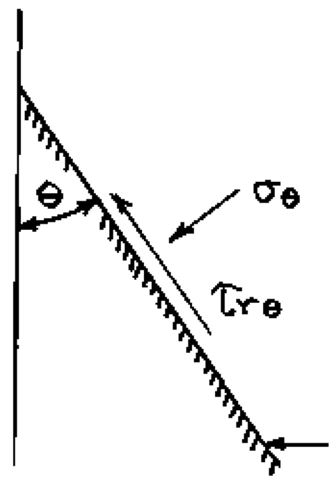

FIGURE 2-6. FORCES ON RIGID SURFACE MOVING THROUGH SOIL

In the case where the wall or surface is moving into the soil, the passive case will be considered and thus only the positive case will be used. That is,

$$\tau_{r\theta} = \sigma_\theta \tan \delta \tag{2.5}$$

2.3.3 <u>The Stress Function</u>

To facilitate the solution of the system of equations which describes the problem, we introduce a dimensionless stress function $S(\theta)$ defined as

$$\sigma = \rho g r S(\theta) \tag{2.6}$$

where: σ is the mean stress at a point,

$$= \frac{\sigma_1 + \sigma_3}{2}$$

σ_1 and σ_3 are the major and minor principal stresses respectively.

It is seen that the stress function relates the stress at a point to the density of the material and also to the spatial position of that point in relation to the origin of coordinates. The use of $S(\theta)$, enables equations (2.2) and (2.3) to be expressed in a form which is readily amenable to analysis, thus constituting a similarity variable which enables the stress at any point in the material to be determined. Its determination at various points within a region enables the mapping of the stress distribution throughout the region. Substituting for σ in equation (2.3), we obtain:

$$\sigma_r = \sigma(1 + \sin\phi \cos 2\Psi')$$

$$\sigma_\theta = \sigma(1 - \sin\phi \cos 2\Psi') \qquad (2.7)$$

$$\tau_{r\theta} = \sigma \sin\phi \sin 2\Psi'$$

From equations (2.7), (2.6) and (2.2),

$$\sin\phi \sin 2\Psi' \frac{ds}{d\theta} + 2S \sin\phi \cos 2\Psi' \left[\frac{d\Psi'}{d\theta} + 1\right] + S(1+\sin\phi \cos\Psi') = \cos\theta$$

$$(2.8)$$

$$(1-\sin\phi \cos 2\Psi') \frac{ds}{d\theta} + 2S \sin\phi \sin 2\Psi' \left[\frac{d\Psi'}{d\theta} + 1\right] + S \sin\phi \sin 2\Psi' = -\sin\theta$$

From equations (2.8), we obtain:

$$\frac{d\Psi'}{d\theta} = \frac{\cos\theta - \sin\phi \cos(2\Psi' + \theta) - S\cos^2\phi}{2S\sin\phi(\cos 2\Psi' - \sin\phi)} - 1$$

$$(2.9)$$

$$\frac{dS}{d\theta} = \frac{S \sin 2\Psi' - \sin(2\Psi' + \theta)}{\cos 2\Psi' - \sin\theta}$$

A solution of equation (2.9) requires the specification of boundary conditions along the surfaces OB and OC shown in Figure 2-2.

2.3.4 Boundary Conditions

Since Region I in Figure 2-7 represents a Rankine Passive zone, the boundary conditions along OC may be readily specified. The boundary conditions at point C (Sokolovski, 1960, Harr, 1966) are:

$$S = \frac{\cos\theta}{1 - \sin\phi}$$

$$\psi' = \frac{\pi}{2} - \theta \qquad (2.10)$$

where: $\theta = \frac{\pi}{4} + \frac{\phi}{2}$

Substituting for θ, we obtain:

$$S = \frac{\cos\left(\frac{\pi}{4} + \frac{\phi}{2}\right)}{1 - \sin\phi}$$

and (2.11)

$$\psi' = \frac{\pi}{4} - \frac{\phi}{2}$$

The second of equations (2.11) may be derived directly from the knowledge that the major principal stress acts in a horizontal direction in Region I.

Since the boundary conditions at point B and along the boundary OB (in Figures 2-2 and 2-7) are in no way defined, and recalling that equation (2.5) describes the stress conditions at the rigid wall-soil interface, the assumption that the mass in zone O'ABO in Figure 2-2 is rigid provides one with the knowledge that the direction of the major

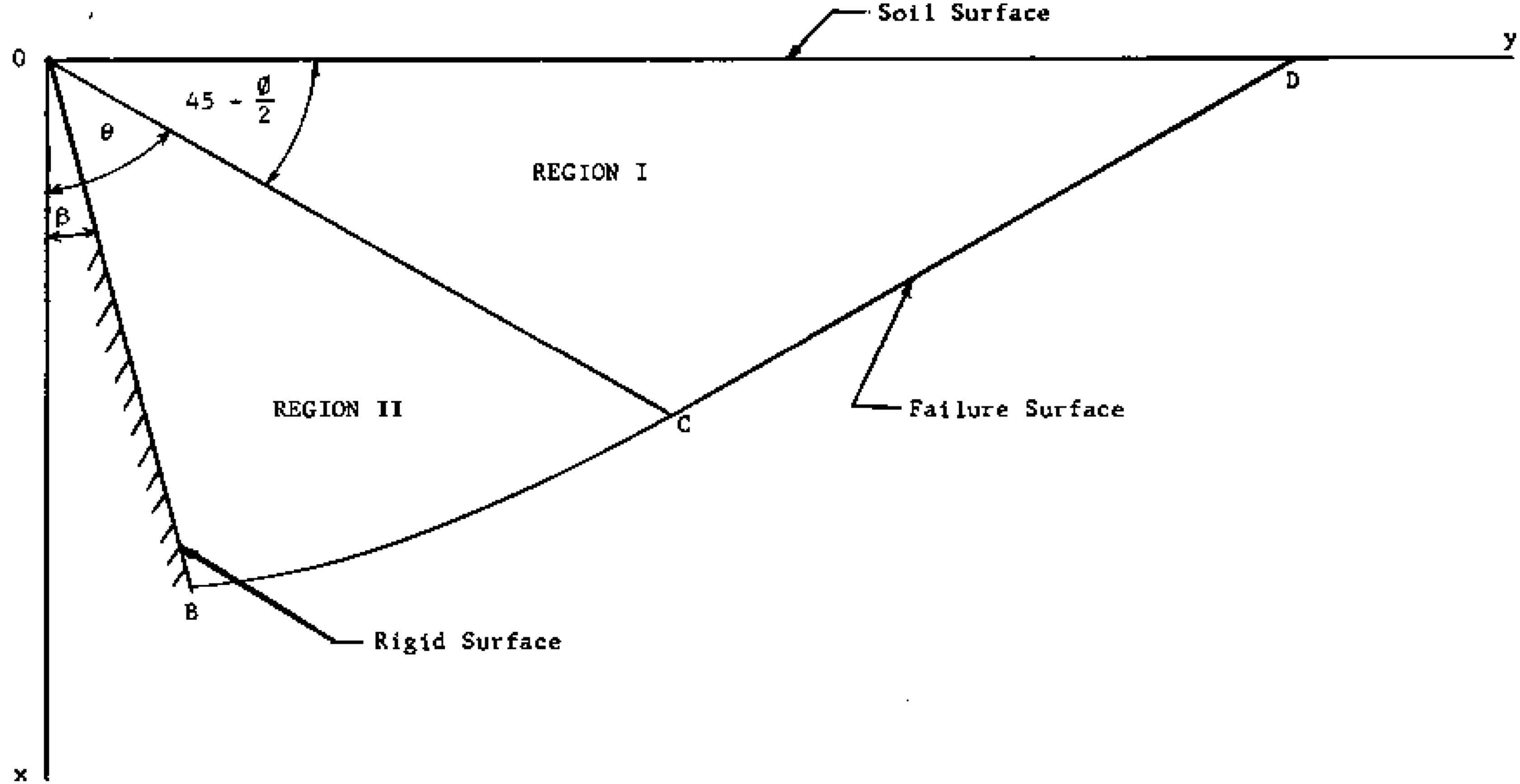

FIGURE 2-7. PROPOSED ANALYTICAL MODEL OF FAILURE CONFIGURATION FOR DESCRIPTION OF BOUNDARY CONDITIONS

principal stress will be constant throughout this region. Thus the determination of ψ' at point A will be sufficient for the determination of ψ' at B.

Substituting equation (2.7) into equation (2.5), we obtain:

$$\sin \phi \sin 2\psi'_B = \left[(1 - \sin \phi \cos 2\psi'_B)\right] \tan \delta$$

Hence:

$$\sin \phi \sin 2\psi'_B \cos \delta = \sin \delta - \sin \phi \cos 2\psi'_B \sin \delta$$

$$\sin \phi \sin (180 - 2\psi'_B) \cos \delta = \sin \delta \quad \sin \phi \cos (180 - 2\psi'_B) \sin \delta$$

Therefore:

$$\sin \phi \left[\sin (180 - 2\psi'_B) \cos \delta - \cos (180 - 2\psi'_B) \sin \delta\right] = \sin \delta$$

$$\sin (180 - 2\psi'_B - \delta) = \frac{\sin \delta}{\sin \phi}$$

We thus obtain:

$$\psi'_B = 0.5 \left[\pi - \delta - \arcsin \frac{\sin \delta}{\sin \phi}\right] \qquad (2.12)$$

where ψ'_B is the angle of inclination of the principal stress direction to the θ-axis at point B.

To determine the stress function S_B, at point B, we employ an iterative solution (Runge-Kutta Method), as follows:

1. estimate a value of S_B
2. by a process of numerical integration, work from point A to point C
3. compare the value of S_C as determined above with the value calculated from equations (2.12). If the difference is too large, estimate a new value of S_B and repeat the procedure.

By repeating the procedure until the two values of S_C obtained from equations (2.11) and by calculation agree to within 0.01, the true value of S_B is obtained. The results of this computation are summarized in Figures 2-8 and 2-9, which show the variation of ψ' and S with θ respectively, for various values of the angle β.

2.4 GEOMETRY OF THE FAILURE SURFACE

To obtain a complete solution of the rigid wall-soil interaction problem, we require the determination of the shape of the failure surface. From the experiments, it was observed that lines AB and CD in Figure 2-2 were straight, which is consistent with the assumption that zones O'ABO and OCD represent a rigid and a Rankine zone respectively. Since these are regions of constant state it is thus only necessary to specify the equation of the spiral curve represented by BC in Figure 2-2.

The solution to this part of the problem may be sought through the use of the method of characteristics. We recall that a characteristic is defined as a line along which discontinuities in derivatives propagate or across which derivatives of the first or second order, or both, are discontinuous. On consideration of the Equations of Variation of the present system, given as equations (2.9), it will be seen that the derivatives of ψ' and S become discontinuous when

$$\psi' = \pm\left(\frac{\pi}{4} - \frac{\phi}{2}\right)$$

or

$$\psi' = \pm\mu \tag{2.13}$$

$$2\mu = \frac{\pi}{2} - \phi$$

We note that when $\psi' = \pm\mu$ in equations (2.9), the denominators of these equations vanish. The numerators may simultaneously vanish or

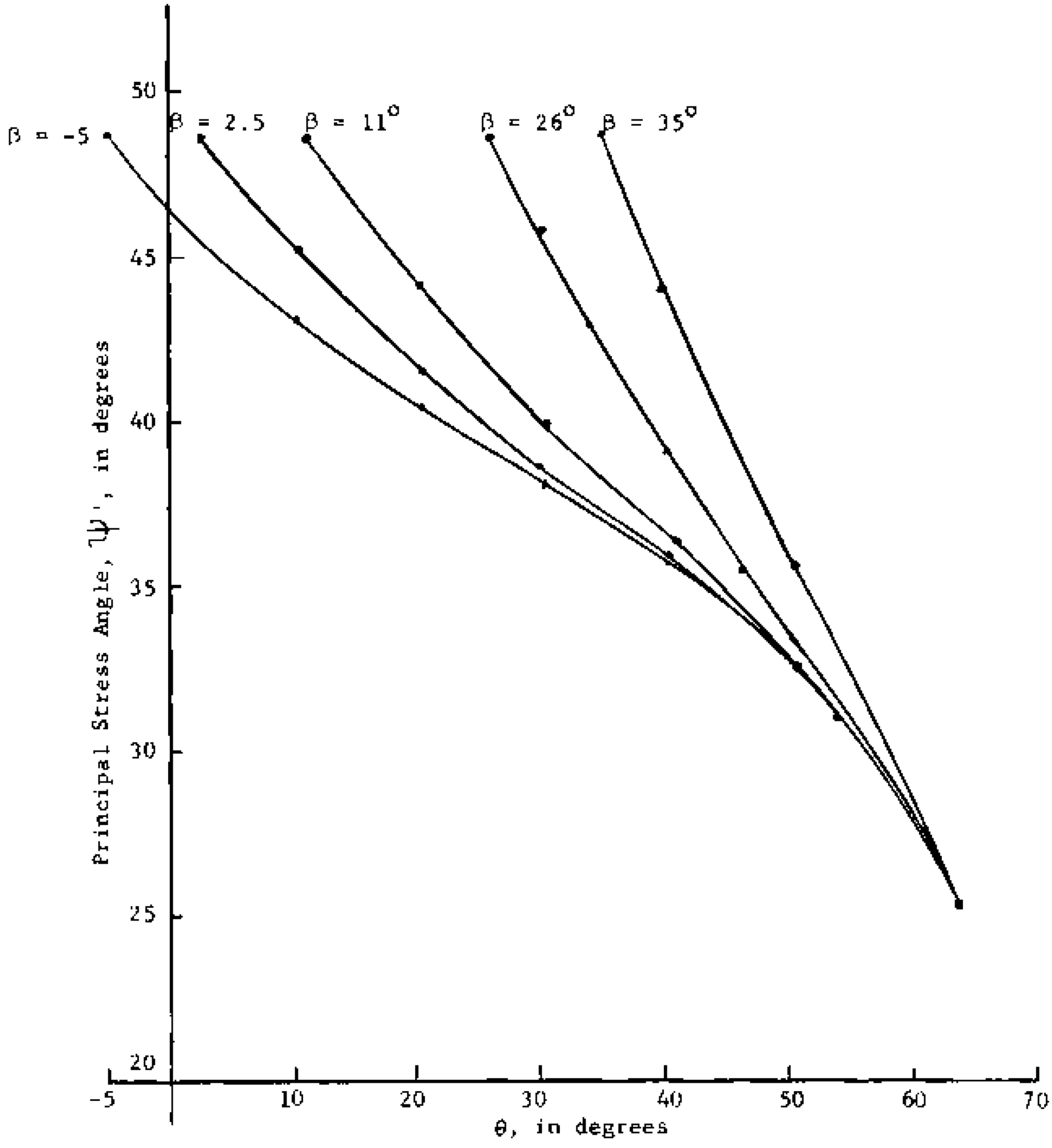

FIGURE 2-8. PLOT OF PRINCIPAL STRESS ANGLE $\psi'(\theta)$ VERSUS (θ) AS A FUNCTION OF β

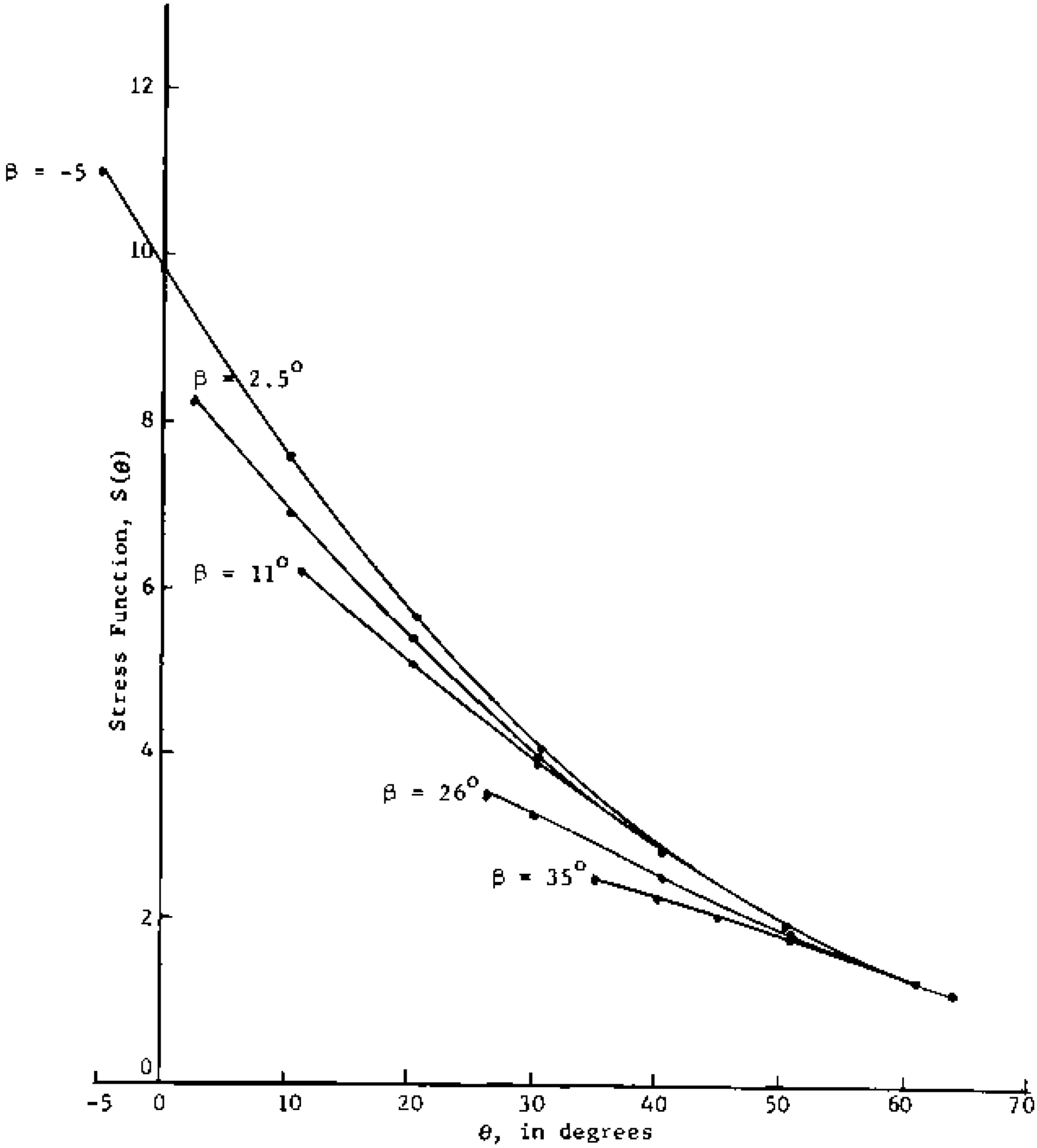

FIGURE 2-9. PLOT OF STRESS FUNCTION, $S(\theta)$ VERSUS θ AS A FUNCTION OF β

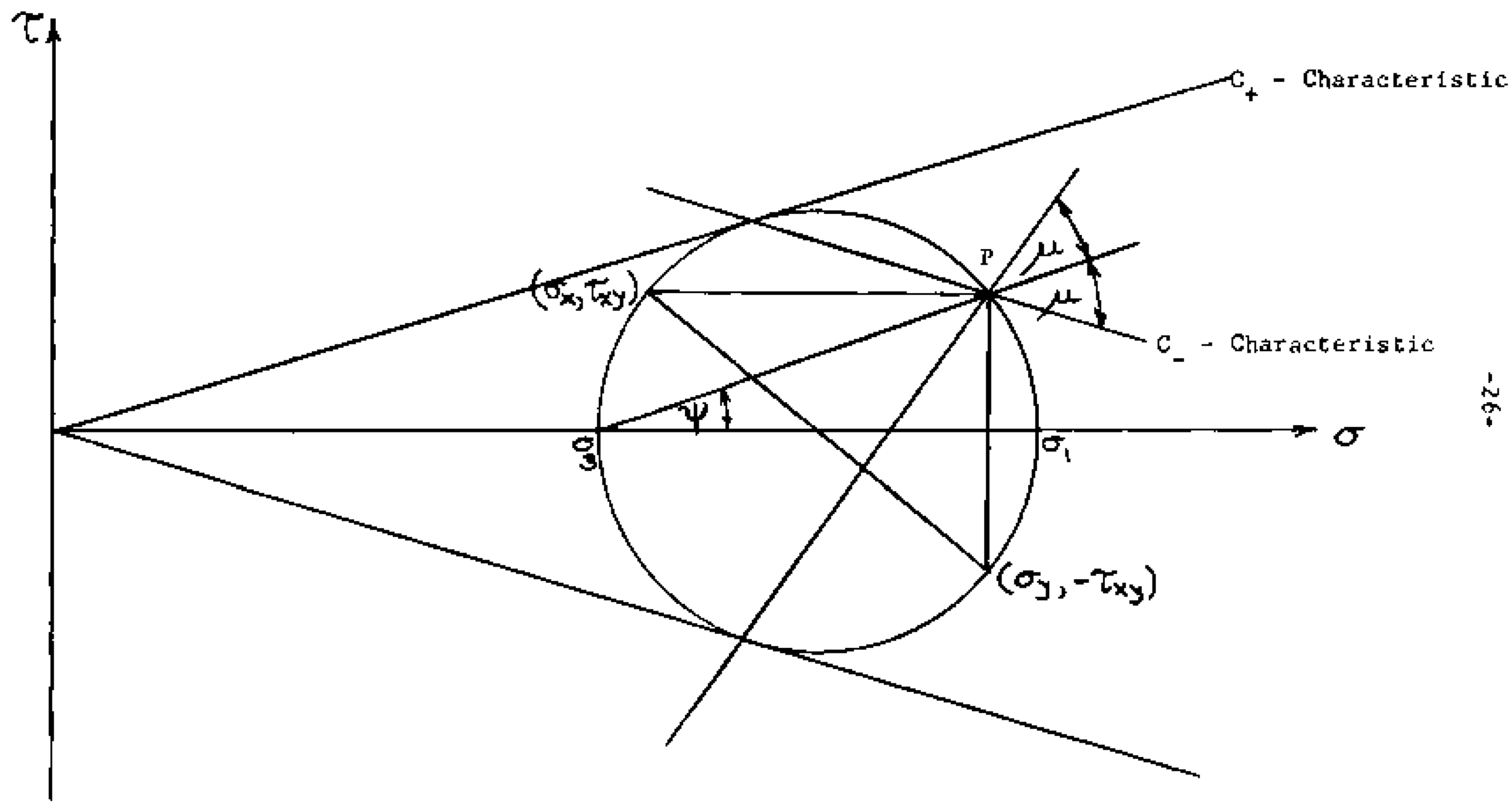

FIGURE 2-10. GEOMETRY OF SLIP LINES IN MOHR PLANE

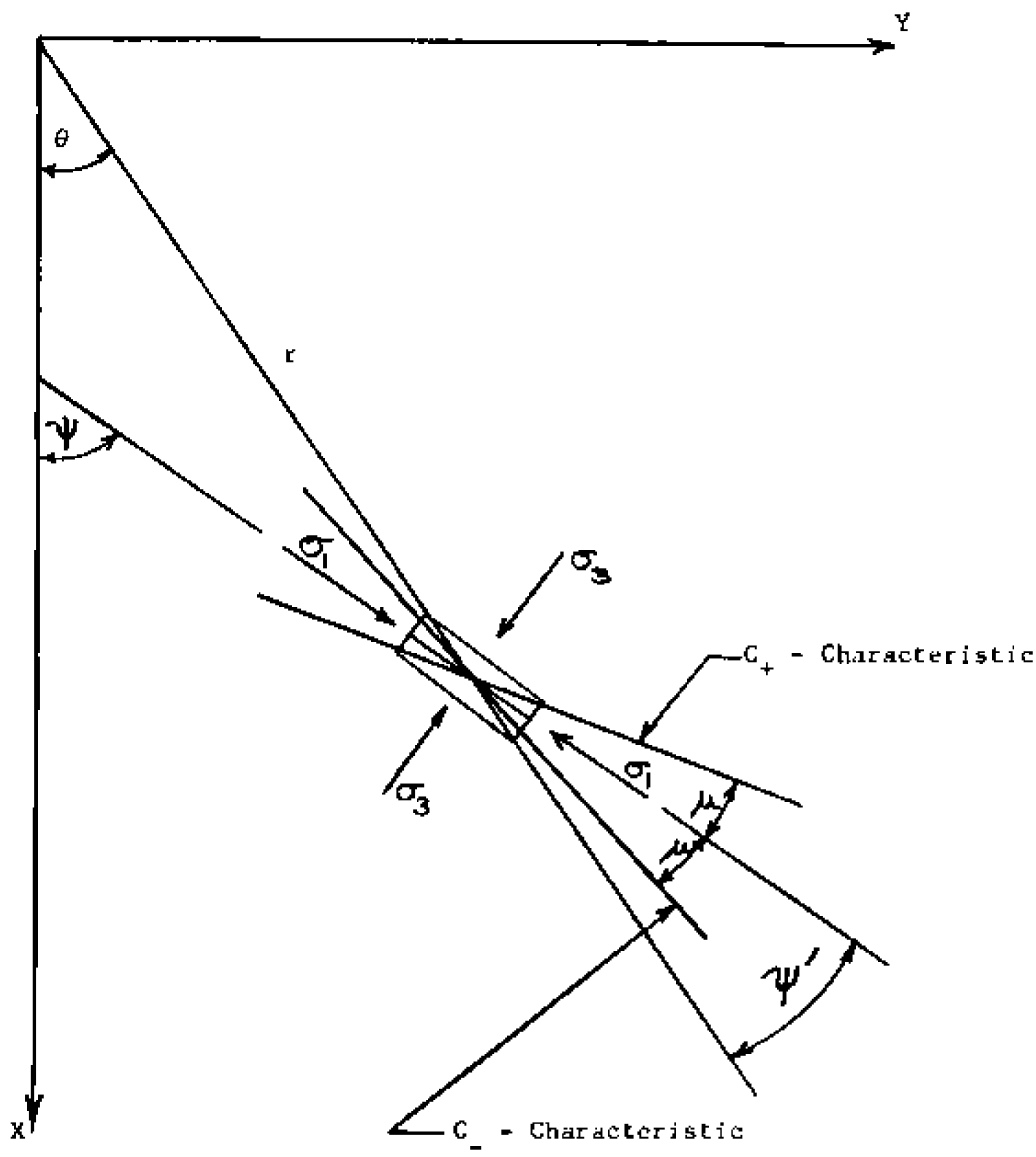

FIGURE 2-11. GEOMETRY OF SLIP LINES IN THE PHYSICAL PLANE

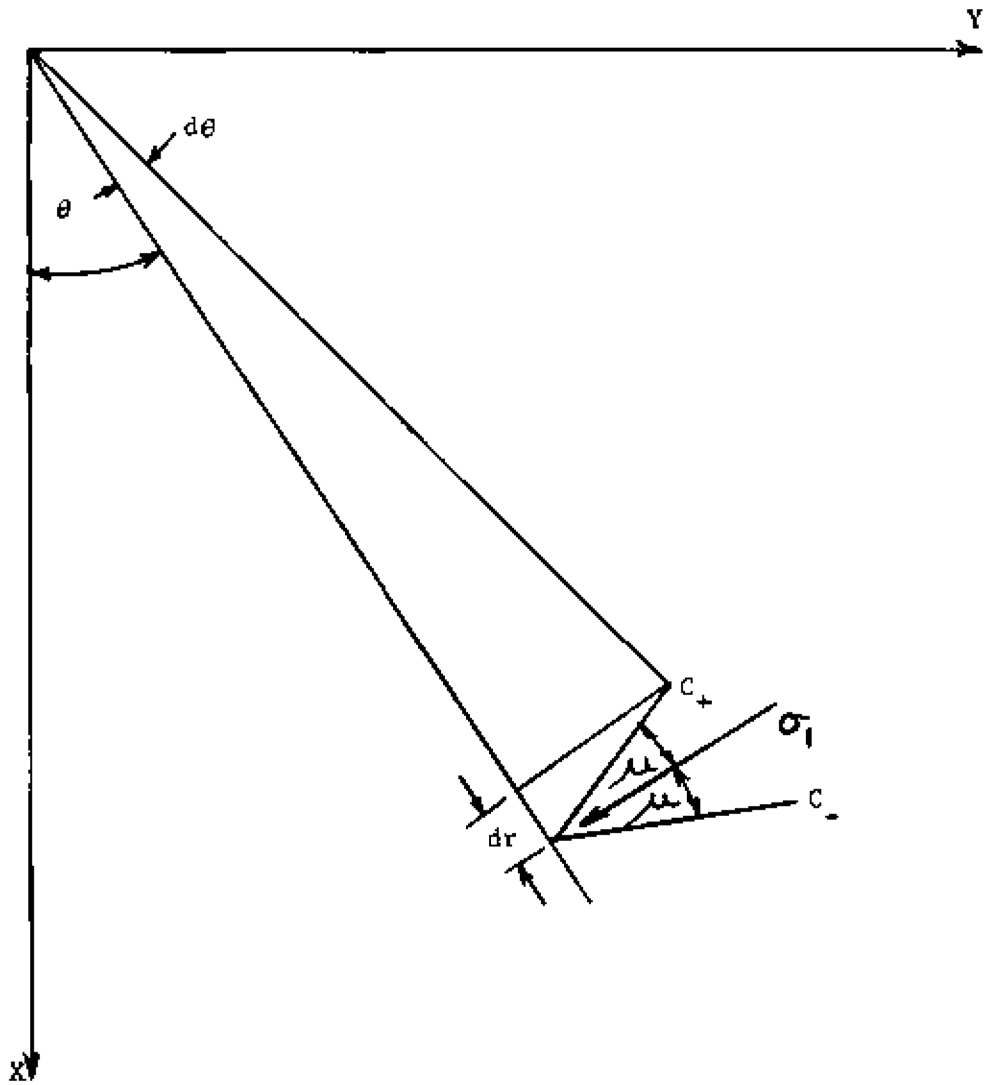

FIGURE 2-12. INCREMENT ALONG RADIAL SLIP LINE

may be different from zero. If the numerators vanish, then equations (2.13) define the characteristics of the system. If they are different from zero, equations (2.13) define a line of discontinuity which has been shown to coincide with the slip lines of the system (Harr, 1966). It has been shown that the slip lines form the envelope of the characteristics of any system (Prager, 1953; Harr, 1966) and as such, equations (2.13) define the slip lines of the present system.

The slip lines comprise two families of curves which intersect at an angle of $2\mu = \frac{\pi}{2} - \emptyset$ and are inclined at angles of $\psi' \pm \mu$ to the radius vectors. The geometry of the slip lines in the Mohr plane is shown as Figure 2-10, while the geometry in the physical plane is shown as Figure 2-11.

The equation of the slip lines themselves may be determined from consideration of Figure 2-12. It will be seen that

$$
\begin{aligned}
-\frac{r d\theta}{dr} &= \tan\left[\pi - (\psi' \pm \mu)\right] \\
\frac{r d\theta}{dr} &= \tan(\psi' \pm \mu) \\
\int_{r_o}^{r_\theta} \frac{dr}{r} &= \int_o^\theta \cot(\psi' \pm \mu)\, d\theta \\
r_\theta &= r_o \exp\left[\int_o^\theta \cot(\psi' \pm \mu)\, d\theta\right] \\
&= r_\beta \exp\left[\int_\beta^\theta \cot(\psi' \pm \mu)\, d\theta\right] \qquad (2.14)
\end{aligned}
$$

where: r_θ = length of radius vector at angle of θ to initial position

r_β = length of radius vector at initial position

β = angle of inclination of surface OB (Figure 2-2) to vertical.

The equation of the C_+ characteristic, which defines the failure surface is given by

$$r_\theta = r_\beta \exp\left[\int_\beta^\theta \cot(\psi' + \mu)\, d\theta\right]$$

$$\mu = \frac{\pi}{4} - \frac{\phi}{2} \qquad (2.15)$$

Equations (2.15) may be solved by a process of numerical integration, utilizing Simpson's Rule, to yield the failure surface.

2.5 PREDICTION OF HORIZONTAL FORCES

With the determination of the stress function at point B (Figure 2-2) it now becomes possible to determine the horizontal and vertical forces acting along OB. To compute the forces acting on the grouser however, and hence to provide a complete solution to the problem, the stresses acting within zone O'ABO (Figure 2-2) must be estimated. Since no knowledge of the stress distribution within this zone is readily available, we resort to a simple static equilibrium approach as a first order approximation.

Assuming that the vertical force, P, acting on the top of the grouser produces a Coulombic friction force along the failure surface AB, we obtain:

$$T = P \tan \phi \qquad (2.16)$$

acting along AB. The horizontal component T_H will be defined by:

$$T_H = (P \tan \phi) \cos \alpha \qquad (2.17)$$

as shown in Figure 2-13.

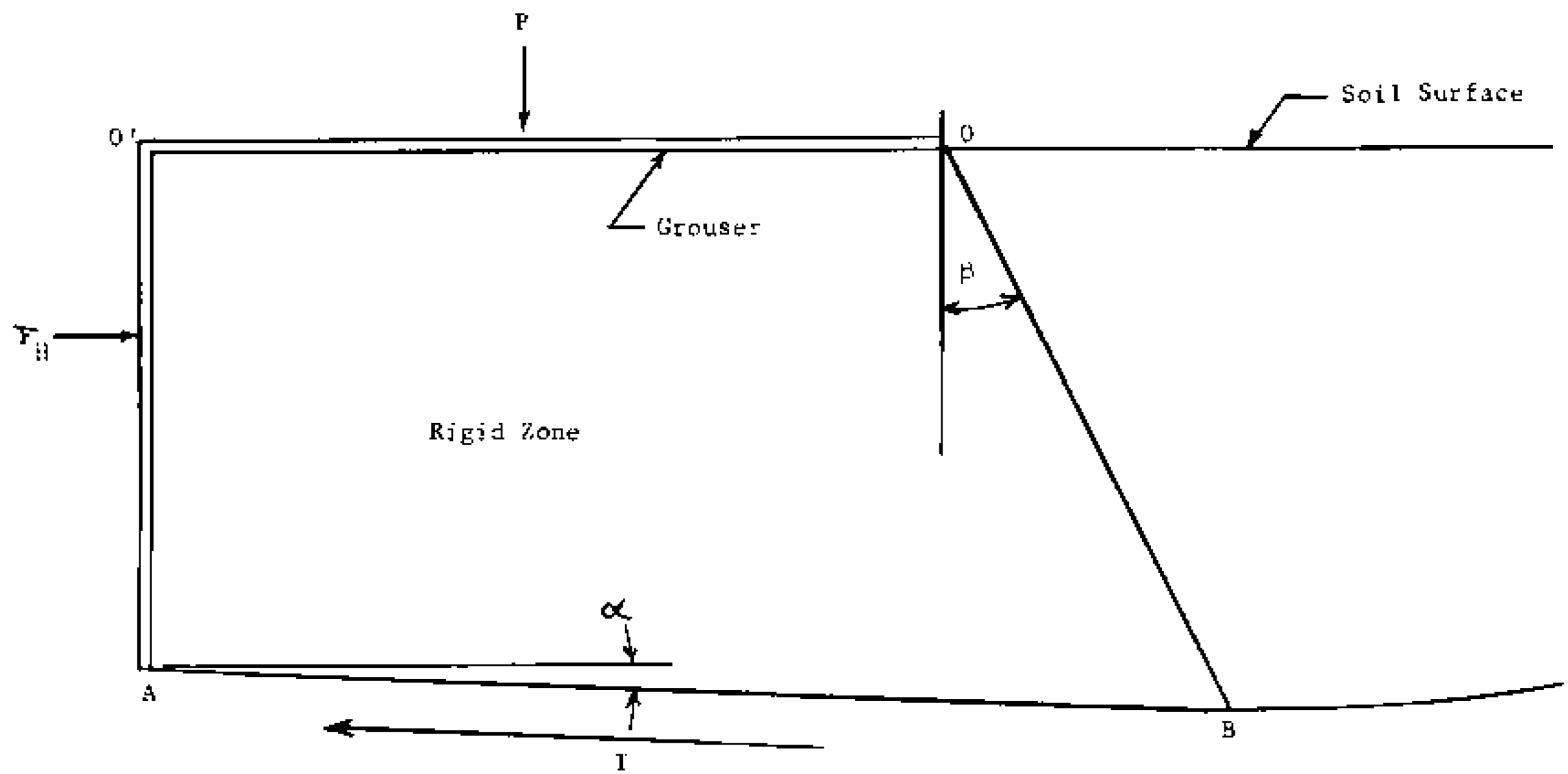

FIGURE 2-13. ANALYTICAL MODEL USED FOR DETERMINATION OF FORCES ACTING IN RIGID ZONE

Taking into account the frictional resistance T_f at the interface of the lucite side-wall and the sand:

$$T_f = kW_1 \tan \delta_L \tag{2.18}$$

where: T_f = frictional force

W_1 = weight of sand within failure zone

δ_L = angle of friction at lucite-soil interface

k = lateral pressure coefficient (taken to be unity for the limit equilibrium case)

An estimate of the angle at which T_f acts may be obtained from experimentation where the mean angle at which the soil moves relative to the horizontal is determined. The resultant force configuration is shown in Figure 2-14.

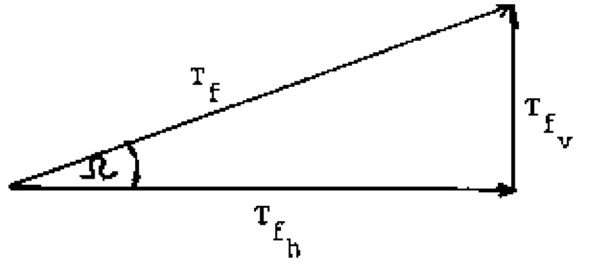

FIGURE 2-14. CALCULATION OF LUCITE-SAND INTERFACIAL FRICTION

From the figure, it will be seen that:

$$T_{f_h} = T_f \cos \Omega$$

$$T_{f_v} = T_f \sin \Omega \tag{2.19}$$

where: T_{f_h} = horizontal component of interfacial friction force

T_{f_v} = vertical component of interfacial friction force

Ω = angle of inclination of mean direction of motion of soil mass to horizontal direction.

CHAPTER 3

APPLICATION OF THEORY

3.1 PRESENTATION OF RESULTS

A summary of the experimental test results is given in Table A-1 in the Appendix. The values of S_B and S_C together with Ψ'_B and Ψ'_C are listed in Table A-2 for the tests for which they were calculated.

Also listed in Table A-2 are the values of β and α for the various tests. In each case, β and α were determined by plotting the displacement patterns of the tests and measuring the experimentally obtained angles.

3.2 PROCEDURE FOR APPLICATION OF THEORY IN EXPERIMENTATION

To demonstrate the theory and its usefulness and applicability in predicting the developed horizontal and vertical forces due to the aggressive action of the grouser, we may consider the following example. Using the basic system parameters for Test Number 9, we have:

Constant vertical load test

ϕ = friction angle of sand = 38°

δ = friction angle at discontinuity OB (i.e., rigid wall) = 29.5°

δ_L = friction angle between sand and lucite wall = 20°

Density = ρg = 100.93 pcf

Width of grouser = 4 inches = b

Grouser dimensions: ℓ = 3 inches
h = 2 inches

Horizontal velocity = 5.25 inches/second

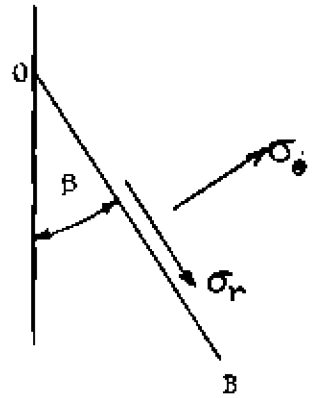

FIGURE 3-1.

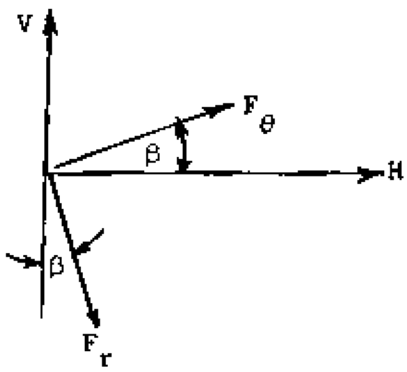

FIGURE 3-2.

We note that the friction angle δ at the discontinuity OB (i.e., rigid wall) is different from ϕ, the friction angle of the sand. The rationale for this may be found in terms of:

a) the assumption of a rigid mass O'ABO originally explained in Chapter 2. It is assumed that the properties at OB are carried over from O'A.

b) if $\delta = \phi$ it will be obvious that the radial zone will no longer exist. Experimentation shows that this cannot be true, i.e., the radial zone (zone OBC in Figure 2-2) does exist.

To complete the specification of the system parameters, it now remains to obtain α, β and thereby compute the length of OB. We note that the length of OB is r in Figure 3-1.

From control tests such as those reported in Table A-1, we may experimentally determine α and β. In Figures 3.3 and 3.4, variations in β due to ℓ/h ratio and also due to velocity are given. Similar graphs may be drawn for α. Thus with this kind of information, it becomes possible to specify α and β and thus compute r, the length of OB (see Figure 2-2 for physical description of α, β and OB).

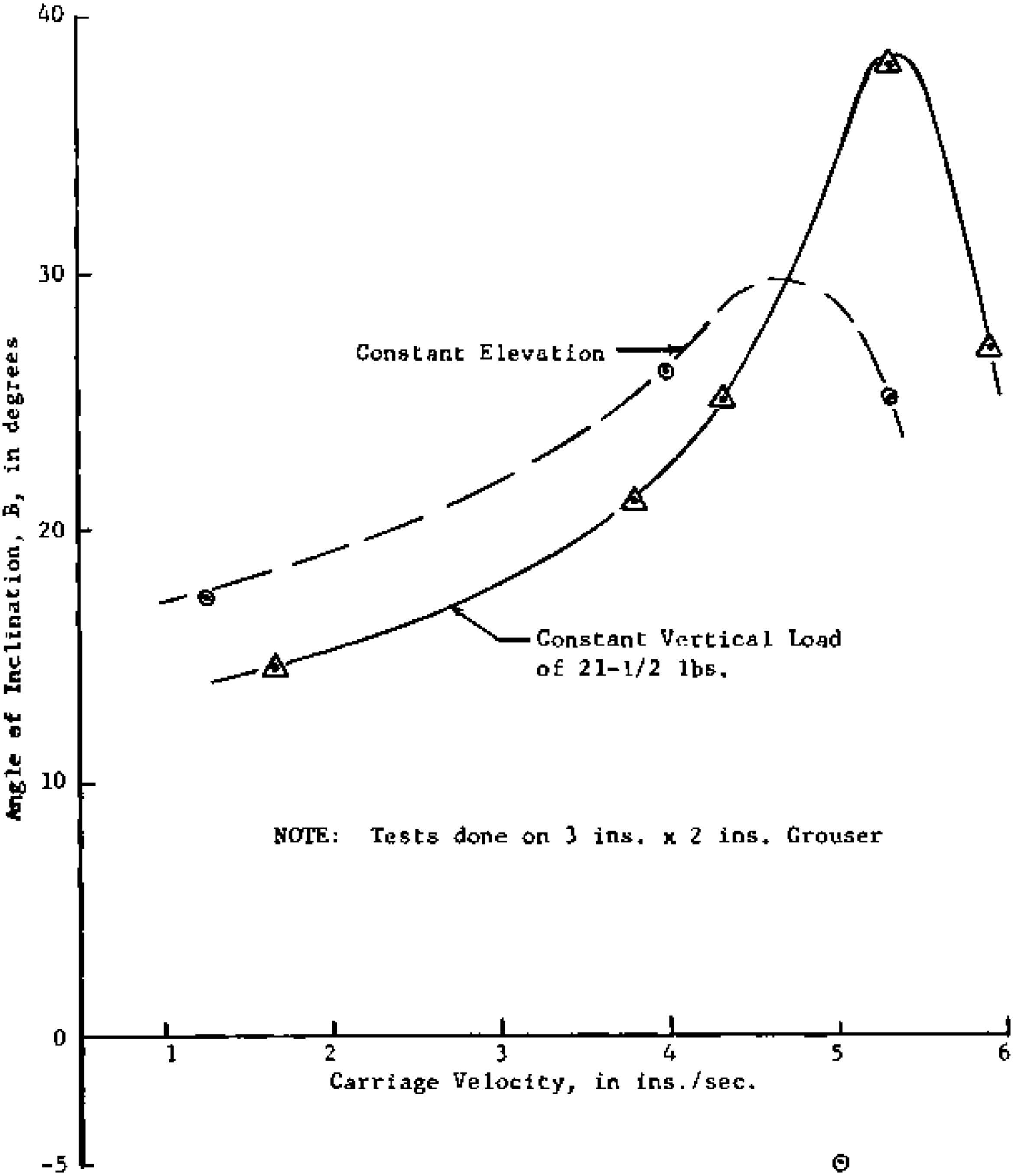

FIGURE 3-3. INFLUENCE OF CARRIAGE VELOCITY ON MEASURED VALUES OF β FOR CONSTANT VERTICAL LOAD AND FOR CONSTANT ELEVATION TESTS

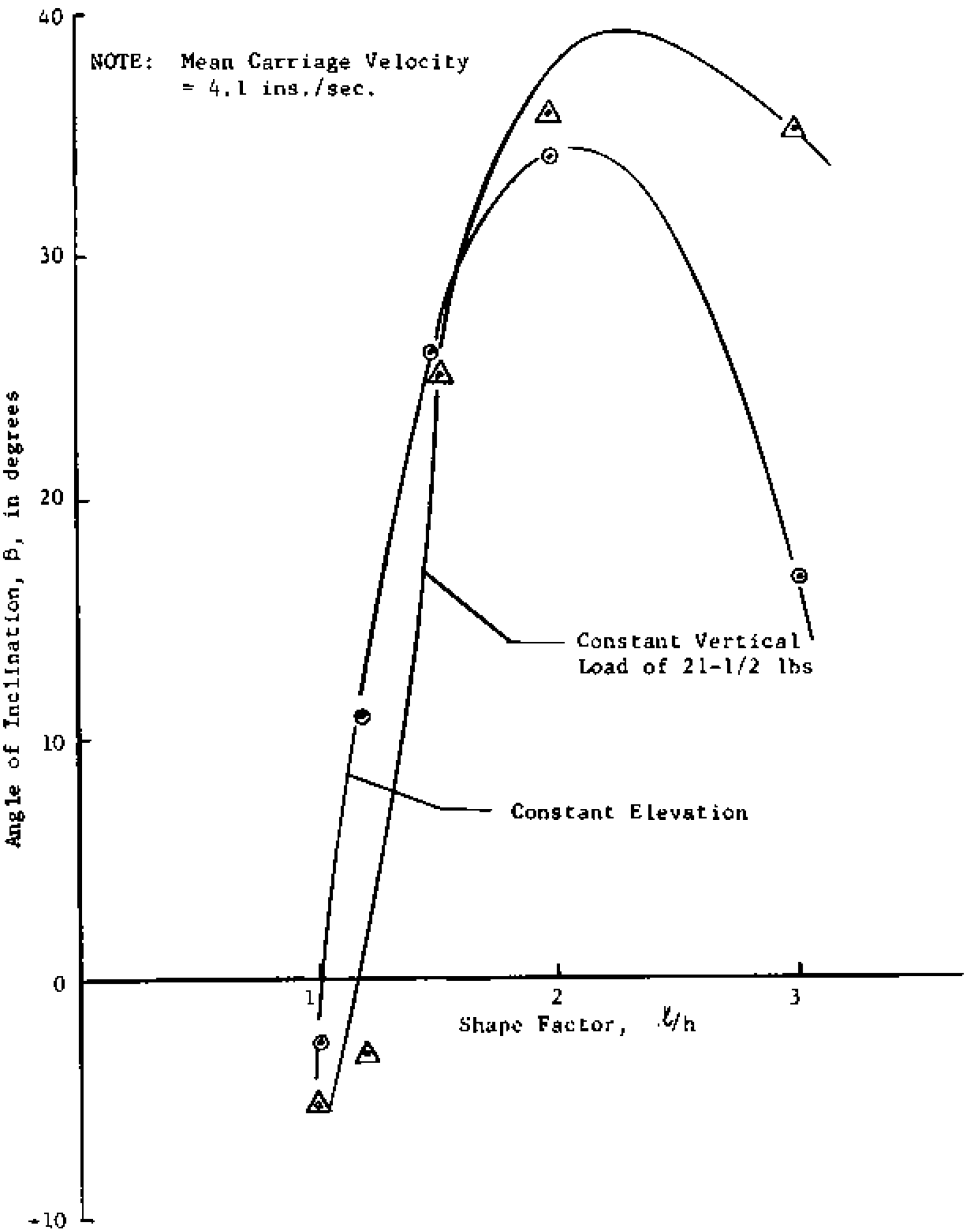

FIGURE 3-4. INFLUENCE OF GROUSER GEOMETRY ON MEASURED VALUES OF β, FOR CONSTANT ELEVATION TESTS

Thus: for a velocity of 5.25 inches/second, we will obtain:

$\beta = 38.0^{\circ}$

$\alpha = -2.5^{\circ}$

$r = 2.28$ inches $= 0.19$ feet

Proceeding with the application of the theory, we now determine values for S_B and ψ'_B. This is accomplished by noting that solution of equations (2.9) in Section 2.3.3, together with the boundary conditions given as equations (2.11) and (2.12) will yield values of the stress function S_B and principal stress angle ψ'_B at point B (Figure 2-2). Alternatively, we can make use of Figures 2-8 and 2-9 to obtain a graphical determination of ψ'_B and S_B. We thus obtain,

$S_B = 2.200$

$\psi'_B = 48.69^{\circ}$

From equations (2.7) in Section 2.3.3

$$\begin{aligned} \sigma_r &= \sigma(1 + \sin\phi \cos 2\psi') \\ \sigma_\theta &= \sigma(1 - \sin\phi \cos 2\psi') \end{aligned} \tag{3.1}$$

We note from equation (2.6) in Section 2.3.3,

$$\sigma = \rho g r S \tag{3.2}$$

Substituting (3.2) into (3.1) yields,

$$\sigma_r = \rho g r S(1 + \sin\phi \cos 2\psi')$$

$$\sigma_\theta = \rho g r S(1 - \sin\phi \cos 2\psi')$$

Substituting numerical values, we obtain:

$$\sigma_r = 100.93 \times 0.19 \times 2.20 \times 0.92$$

$$= 38.9 \text{ psf}$$

$$\sigma_r = 0.27 \text{ psi}$$

Similarly,

$$\sigma_\theta = 0.316 \text{ psi.}$$

Since the value of S varies linearly between 0.0 at point O and 2.20 at point B in Figure 2-2, the forces may be found from:

$$F_r = \frac{r\,\sigma_r}{2}\,b \tag{3.3}$$

where: b is the width of the grouser.

Similarly,

$$F_\theta = \frac{r\,\sigma_\theta}{2}\,b \tag{3.4}$$

Putting numerical values of r and b into equations (3.3) and (3.4) yields,

$$F_r = (0.27)(4.56) = 1.23 \text{ lbs}$$

$$F_\theta = (0.316)(4.56) = 1.44 \text{ lbs}$$

From consideration of Figure 3-2, it will be seen that

$$F_H = F_{r_H} + F_{\theta_H}$$

$$= F_r \sin\beta + F_\theta \cos\beta$$

Thus: $$F_H = 1.23 \sin 38 + 1.44 \cos 38$$

$$= 1.89 \text{ lbs}$$

To account for the shear force due to the applied vertical load of 21-1/2 lbs, the failure surface for the particular experimental constraints may be determined using equation (2.15) in Section 2.4. We thus obtain the weight of soil in zone O'ABO (Figure 2-2) = 1.66 lbs. With reference to equation (2.17) and Figure 2.13,

$$\text{total vertical weight} = 21.5 + 1.66$$

$$= 23.16 \text{ lbs}$$

Therefore:

$$T_H = (23.16 \tan \phi) \cos \alpha$$

$$= (23.16)(0.78)(0.998)$$

$$= 18.2 \text{ lbs}$$

Finally, account must be taken of the side friction forces. From the theoretically predicted failure configuration using equation (2.15), the total weight of soil in the failed mass may be found to be

$$W_1 = 3.0 \text{ lbs}$$

Thus, from equations (2.18) and (2.19) we obtain:

$$T_{f_h} = 1.09 \text{ lbs}$$

The theoretically predicted total horizontal force, H, is thus given by

$$H = F_H + T_H + T_{f_h}$$

$$= 1.89 + 18.2 + 1.09$$

$$= 21.18 \text{ lbs}$$

We note from Table A-1 in the Appendix that the measured value for H for Test 9 was 22.30 pounds - as compared to the theoretically predicted value of 21.18 pounds. It is thus evident that some measure of success in prediction has been achieved. Table 3.1 shows the comparison between predicted and measured values of the horizontal force H.

3.3 GENERAL APPLICATION OF THEORY

We note that the experimental constraints associated with plane strain generation creates side friction forces between soil and test container. In the event that this can be obviated, the total horizontal force H predicted would no longer need to account for the term T_{fh}. Thus:

$$H = F_H + T_H$$

In three dimensional problems - as would be encountered in field application, empirical modifications (possibly in the form of introduced coefficients) would be necessary in view of the horrendous complexities arising in the solution of the equations in three dimensional form. (The problem of statement of boundary conditions in the three-dimensional problem can be equally difficult.)

TABLE 3.1

COMPARISON OF MEASURED AND CALCULATED HORIZONTAL FORCES FOR ALL TESTS IN WHICH COMPUTATIONS WERE CARRIED OUT

Test No.	Density (pcf)	S_B	Ψ'_B	H (lbs) Measured	H (lbs) Calculated	% Error
8	98.73	3.450	48.69	25.38	22.37	13.40
9	100.93	2.200	48.69	22.30	21.20	4.90
11	100.25	5.400	48.69	19.30	19.50	1.00
13	100.48	6.200	48.69	18.20	15.60	14.30
14	102.20	2.300	48.69	28.40	29.87	5.00
16	101.60	4.650	48.69	53.40	49.75	6.70
17	100.79	3.725	48.69	21.30	24.81	16.40
20	100.42	3.480	48.69	38.00	36.40	4.40
24	100.90	3.725	48.69	50.70	46.50	7.30
27	100.80	10.900	48.69	45.60	43.80	5.00
28	99.94	5.000	48.69	31.90	32.70	2.50
29	101.41	2.500	48.69	15.50	15.40	3.20
30	100.34	2.760	48.69	24.10	22.00	8.70
32	99.10	6.200	48.69	52.00	50.50	3.00
34	100.60	11.000	48.69	50.50	41.10	18.50
35	100.33	9.900	48.69	80.50	75.50	11.00

$\phi = 38^\circ$; $\delta = 29.5^\circ$

CHAPTER 4

DISCUSSION OF RESULTS

4.1 COMPARISON BETWEEN THEORETICALLY COMPUTED AND MEASURED VALUES

In Figures 4-1 and 4-2 we show comparisons between theoretically predicted and actual measured values for grouser performance. It will be seen that good agreement exists between the experimentally measured and the computed results. The apparent slight discrepancies present lie within the limits of experimantal error (usually 10%). It will be noticed that discrepancies begin to become apparent at larger values of carriage velocity and applied vertical load. These may be due to:

a) neglect of inertia terms in the analysis or theoretical computations,

b) the specific value of δ at the OB discontinuity used in the computations, and

c) the computed failure surface using selected values of α and β from prior experimentation.

In all, it will be seen that $\rho v_x \frac{\partial v_x}{\partial x}$ is sufficiently small for the test constraints and thus can be neglected.

Since the deviations between theoretically computed and measured values are not significant, it would appear that the assumptions associated with b) and c) are adequately tenable (within limits) and thus do not detract from the admissibility of the mathematical model used.

4.2 COMPARISON OF RESULTS WITH RESULTS COMPUTED FROM BEKKER'S EQUATIONS

With reference to Figures 4-1 and 4-2, it will be seen that results computed from Bekker's equations (Bekker, 1960) shown in both

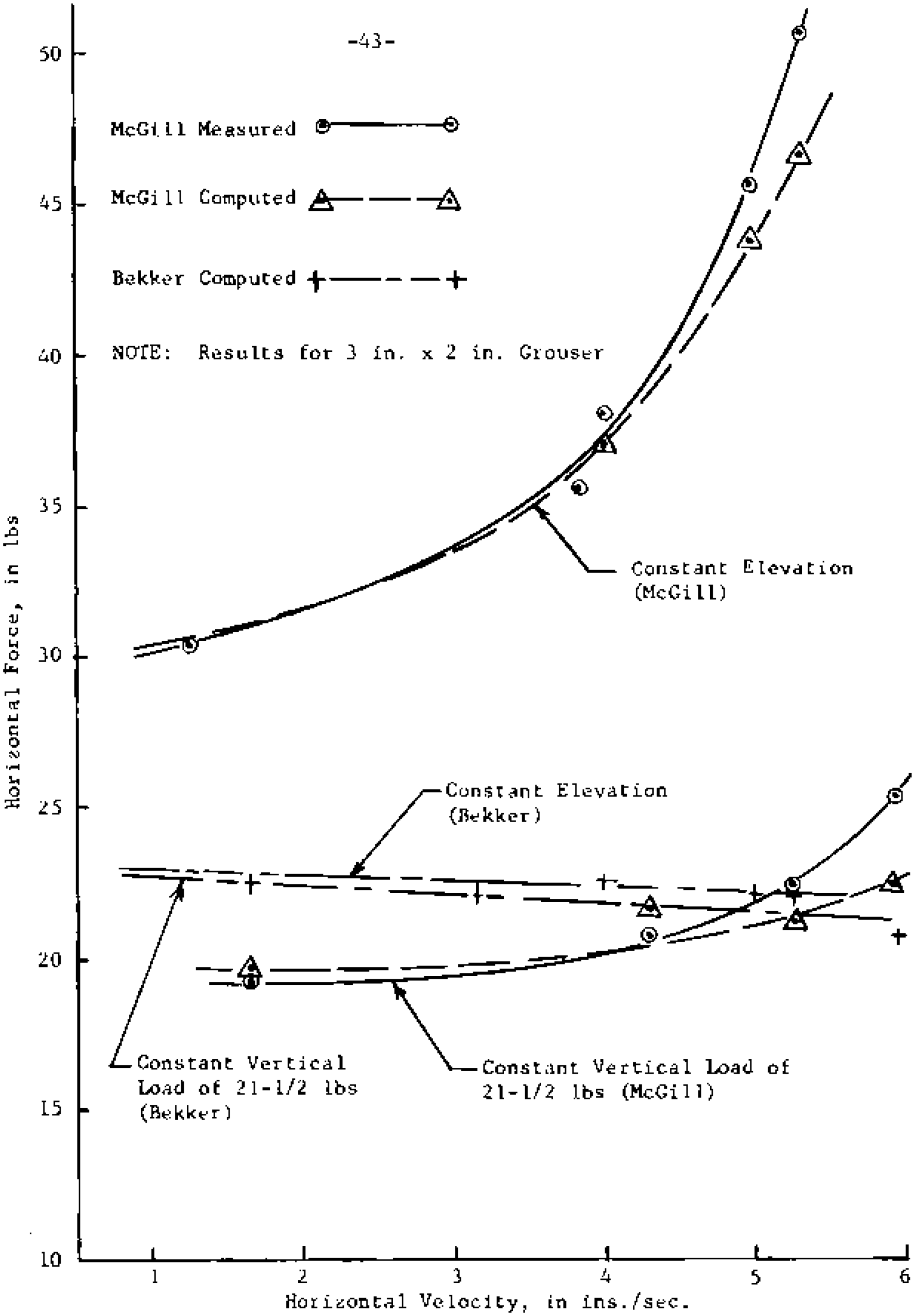

FIGURE 4-1. PLOTS OF PREDICTED AND MEASURED HORIZONTAL FORCES VERSUS HORIZONTAL VELOCITY FOR CONSTANT ELEVATION AND CONSTANT VERTICAL LOAD TESTS

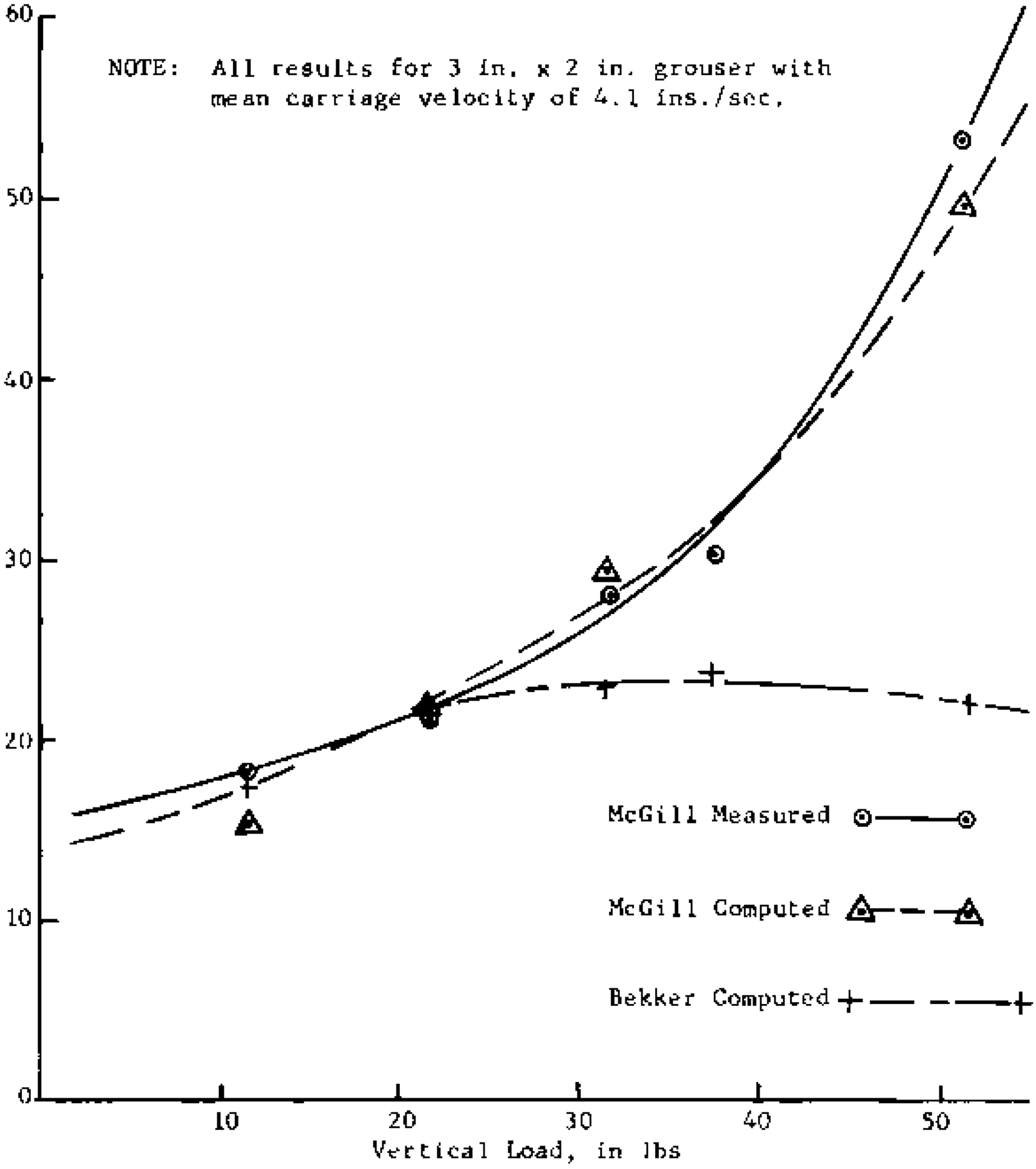

FIGURE 4-2. PLOTS OF PREDICTED AND MEASURED HORIZONTAL FORCES AGAINST APPLIED VERTICAL LOAD

graphs are compared with both the theoretically computed and measured values (McGill results). In the Bekker equations, the horizontal and vertical forces, H and W, are not expressed explicitly in terms of system parameters but rather, are proportional to an angle θ defined by:

$$\theta = \arctan \frac{H}{W}$$

where:

$$H = b(\eta_c \ell c + \gamma \eta_q sz + \gamma \eta_\gamma \ell^2) \sin \theta$$

$$W = b(\eta_c \ell c + \gamma \eta_q sz + \gamma \eta_\gamma \ell^2) \cos \theta \qquad (4.1)$$

b = grouser width

z = sinkage

It is seen that H and W are dependent on such dimensionless trafficability factors as η_q, η_c and η_γ, all of which in themselves are dependent on $\emptyset$, θ and the ratio of ℓ/h.

In view of the above considerations, the two equations for H and W do not permit a direct determination of these forces but instead, must be solved by an iterative process.

The results of these computations are plotted in Figures 4-1 and 4-2 and it will be seen that appreciable deviations occur between the Bekker and McGill results. The results obtained from Bekker's equations are consistent with the definition of the terms used in equations (4.1), and the discrepancies can only be attributed to the assumptions inherent in the derivation of equations (4.1). This derivation assumes an elastic stress distribution beneath the grouser and quasi-static conditions, a fact which will account for the discrepancies between the results shown in Figure 4-2. However, at lower values of vertical load, good agreement between the results obtained from Bekker's equations and from the McGill tests is observed in Figure 4-2.

The computations for the case of the constant elevation tests would appear to be incorrect in the light of the large discrepancies between the Bekker results and the McGill results. This is expected since (in the case of these tests) both the values of H and W must be estimated to arrive at an estimate for θ for the solution of equations (4.1). As a consequence, any comparison between the Bekker and McGill results is meaningless for the constant elevation tests.

In the light of the good agreement between the McGill results and those computed from Bekker's equations however, it can be said with some degree of justification, that Bekker's equations are applicable where the speeds are sufficiently low so that inertia effects may be neglected. If this assumption cannot be made, it would then appear that equations (4.1) are not particularly valid.

4.3 GENERAL

The general discussion following in this and subsequent sections will deal with noticed effects and some of the reasons for these effects.

With reference to Table A-2, it will be seen that the values of S_c and Ψ'_c are in good agreement with those obtained by invoking the Rankine condition at point C (Figure 2-2). The small errors present can be accounted for by the truncation and round-off approximations inherent in machine computations using the Runge-Kutta method.

In all cases, the horizontal forces exerted on the grouser can be thought of as consisting of two parts, one portion due to a change in inertia forces with changes in velocity and weight, and the other portion due to the component provided by the material which is in a state of limiting equilibrium in the radial shear and Rankine zones. With this in mind, the results of this study can be readily explained.

4.4 EFFECT OF CARRIAGE VELOCITY

From Figure 4-1 we note that the developed horizontal force increases slowly with an increase in horizontal velocity up to a value of about 4.5 inches per second. Around this region, the slope of the curve begins to increase fairly rapidly, reflecting a rapid increase in horizontal force with carriage velocity.

Whilst inertia forces (which are proportional to the square of the velocity) increase with increasing velocities, from Figure 3-3 we note that for lower velocities (below 5 inches per second) the angle β, which increases with increasing velocity, will produce decreasing values of calculated resistive forces. Thus the total horizontal force which consists of inertia and resistive forces will increase relatively slowly since the two components are in opposition.

At velocities in excess of 5 inches per second, the value of β begins to decrease, and as a result, the resistive force component resulting from the soil in the radial shear and Rankine zones will tend to increase. The two force components now reinforce each other and the horizontal force will begin to increase rapidly as shown in Figure 4-1. The effect of the velocity induced forces is even more apparent when these results are compared with those shown in Figure 4-2. It will be readily seen that at the low velocities at which these tests were conducted (of the order of 0.014 inches per second), the change in horizontal force with horizontal velocity is not noticeable.

The effect of the carriage velocity on the magnitude of the measured vertical forces is as shown in Figure 4-4. It can be seen that the trend of the curve in this case is similar to that which describes the variation of horizontal force with velocity (Figure 4-1). As mentioned previously, no computed values of vertical forces are available in view of the lack of knowledge of the stress distribution in the soil immediately beneath the grouser.

4.5 EFFECT OF APPLIED VERTICAL LOAD

In the case of the variation of the horizontal forces with applied vertical load, the increase in generated horizontal force with an increase in vertical load, shown in Figure 4-2, is consistent with the concept of an increase in shear strength with an increase in confining or overburden pressure. In comparing Figure 4-2 with Figure 4-5 for constant vertical load tests at very low speeds (of the order of 0.014 inches per second), a marked divergence between the two is observed at large values of applied vertical load.

The divergence can be explained in terms of inertia effects. At high speeds and large values of vertical loads, the momentum forces become significant and will tend to increase the magnitude of the horizontal force. Hence the forces will increase with increasing vertical load, giving a curve which is convex to the axis. At very low speeds however, momentum forces are negligible even at high vertical load levels. Since the angle α, shown in Figure 2-13 tends to increase with increasing vertical load, the horizontal component of shear force along the surface AB (Figure 2-13) will decrease. As such, the rate of increase in horizontal

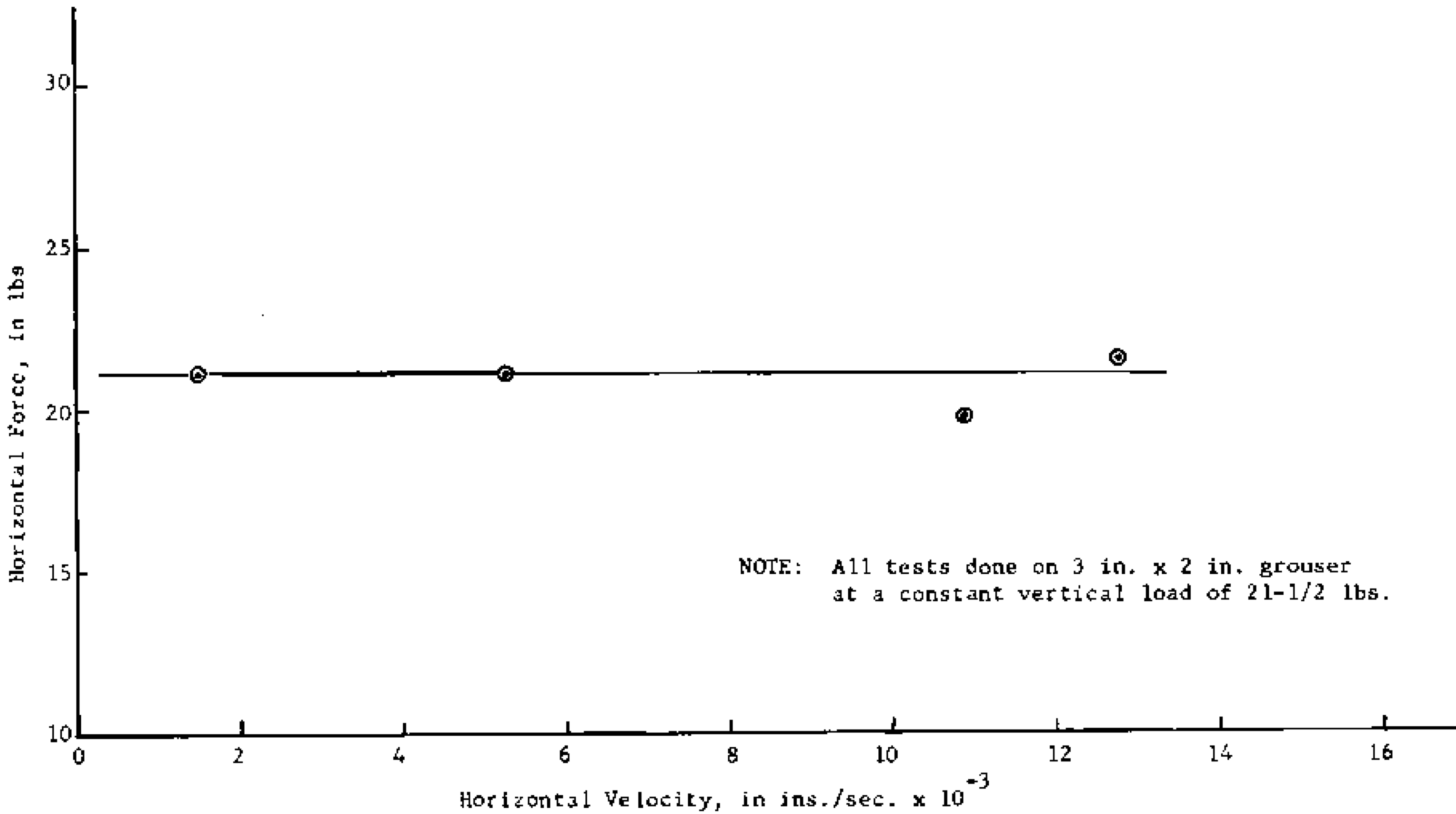

FIGURE 4-3. PLOT OF MEASURED HORIZONTAL FORCE VERSUS HORIZONTAL VELOCITY FOR SLOW TESTS

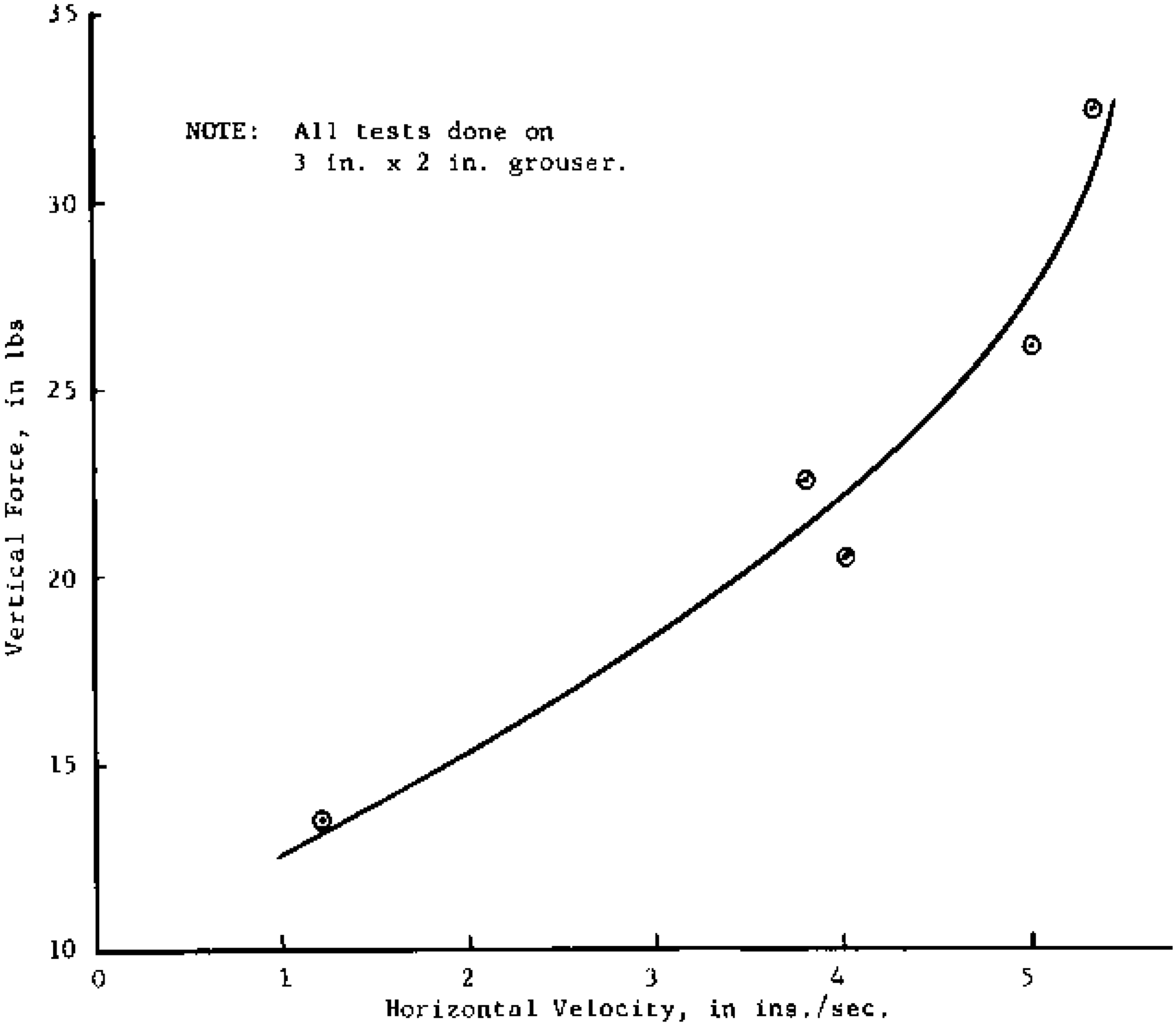

FIGURE 4-4. VARIATION OF MEASURED VERTICAL FORCE WITH HORIZONTAL VELOCITY FOR CONSTANT ELEVATION TESTS

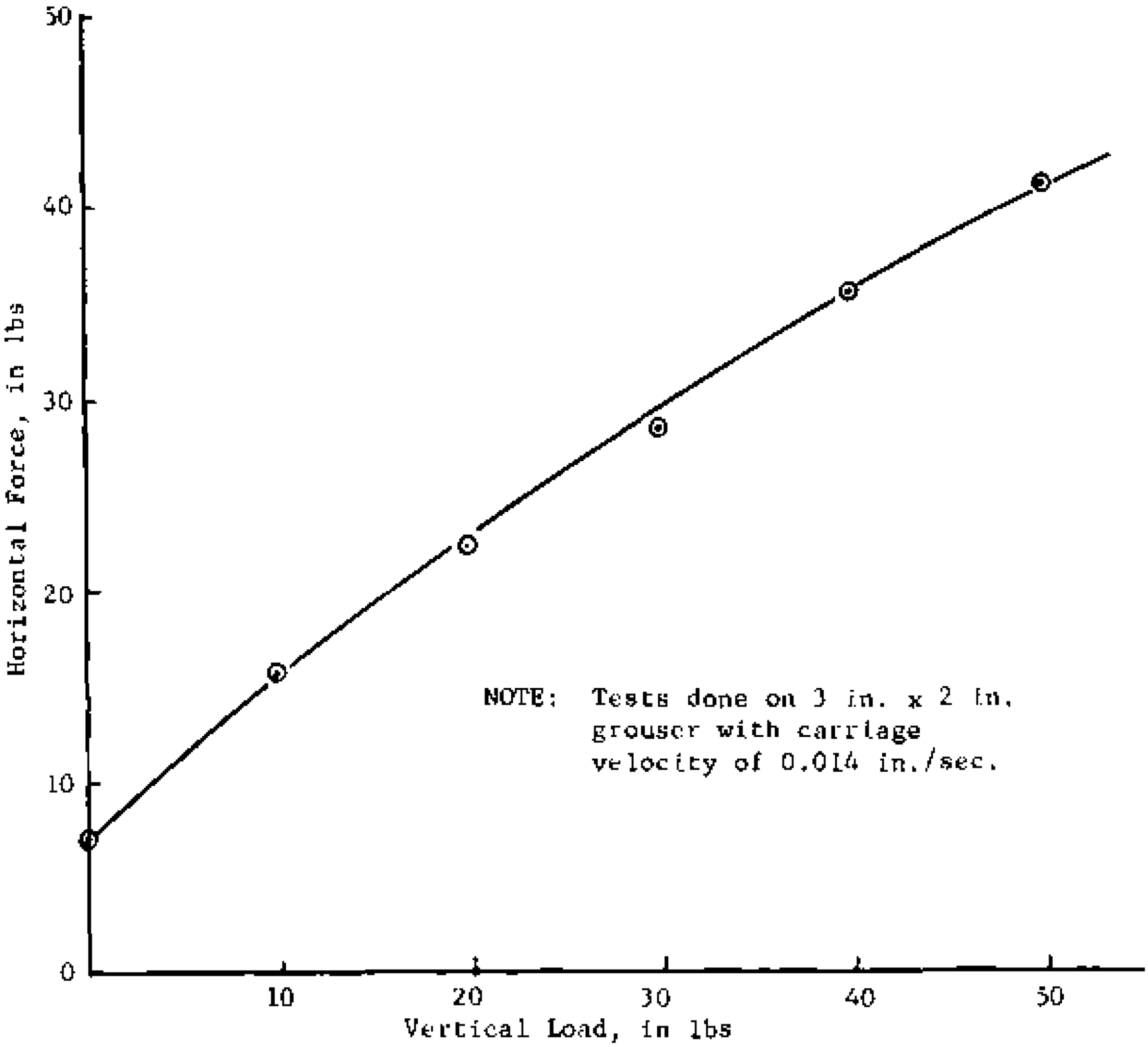

FIGURE 4-5. PLOT OF HORIZONTAL FORCE AGAINST APPLIED VERTICAL LOAD FOR SLOW TESTS

force with increase in vertical load, for the low speed case, will decrease. Consequently, the resulting curve will be concave towards the abscissal axis.

4.6 EFFECT OF GROUSER GEOMETRY

The effect of grouser geometry on performance may be seen in Figures 4-6 and 4-7. It is noted that an excellent correspondance is achieved between theoretically computed and measured values for the constant elevation tests (Figure 4-6). For the constant vertical load tests divergence occurs at low values of ℓ/h.

The variation of horizontal force with shape factor is not solely a result of the increased force produced by the increased contact area. If this were the case, the curves shown in Figures 4-6 and 4-7 would be parabolic in shape since the horizontal force is a function of the square of the depth. It would appear that the curves exhibit a singular point for shape factors in the neighbourhood of 1.7. At this point, the curves change slope rather abruptly, a fact which is emphasized on an examination of Figure 3-4.

In Figure 3-4 we note that the value of β increases rapidly with a decrease in shape factor and reaches a maximum value at a shape factor in the region of 2. This would correspond to a decrease in stress function and hence in horizontal force. As mentioned previously, such a decrease would act in opposition to an increase in force as a consequence of the increase in h. As such, the net horizontal force component will change slowly with increasing h, a fact which is apparent in Figures 4-6 and 4-7. For shape factors below a value of 2.0 however, β decreases rapidly and

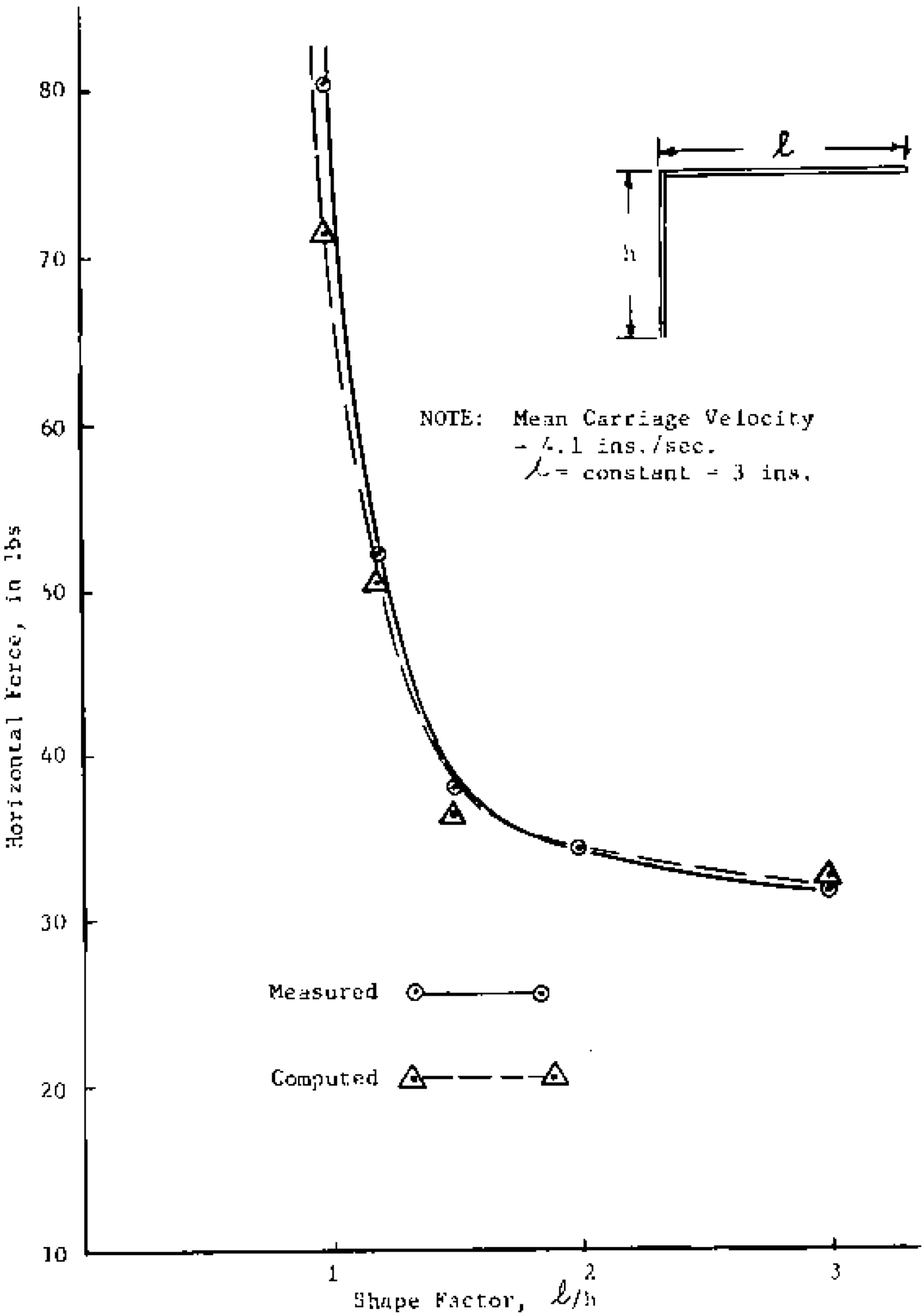

FIGURE 4-6. INFLUENCE OF GROUSER GEOMETRY ON PREDICTED AND MEASURED HORIZONTAL FORCES FOR CONSTANT ELEVATION TESTS

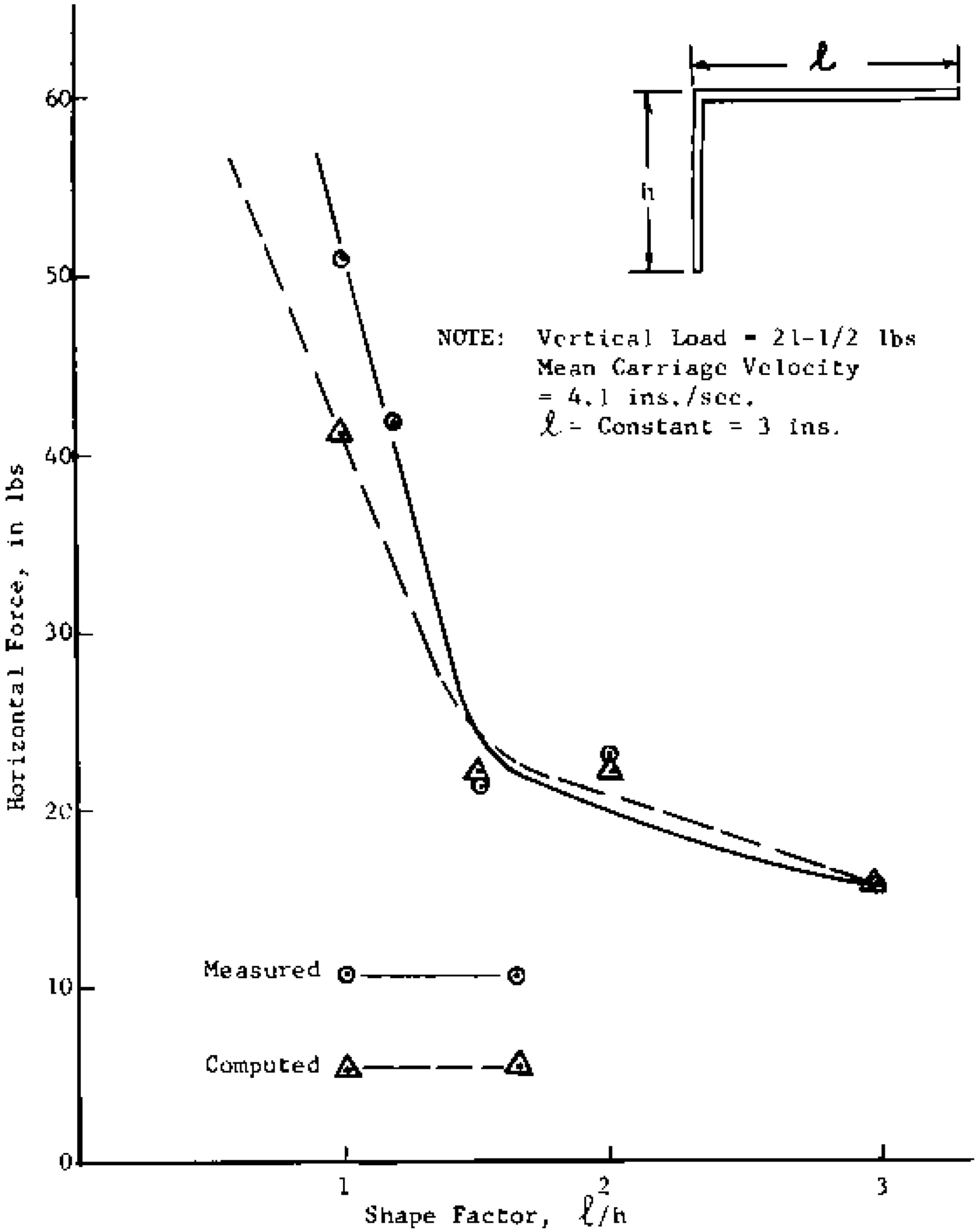

FIGURE 4-7. INFLUENCE OF GROUSER GEOMETRY ON PREDICTED AND MEASURED HORIZONTAL FORCES FOR CONSTANT VERTICAL LOAD TESTS

thus the horizontal force contributed by the radial shear and Rankine zones will increase. Consequently, the force component resulting from an increase in h will be reinforced by the component resulting from the decrease in β and the net horizontal force will begin to increase rapidly. Again, this is apparent on an examination of the figures.

The existence of such a point of singularity is similar to results obtained by Chen (1969) in his study of soil cutting. In this particular case it was found that a minimum value of horizontal force was obtained for an angle of blade inclination of 45 degrees. In the present case of the grouser, it will be seen that the angle β reaches a maximum value, in the region of 35 degrees, at a shape factor in the neighbourhood of 2. This does not correspond to a minimum horizontal force however, since the force consists of two components. It will be recognized that only one of these, the component arising from the soil in the radial shear and Rankine zones, reaches a minimum. The second component, arising from the increased surface area with increasing h, is a monotonic increasing function, and as such, the sum of these two (i.e., the net horizontal force) should continually decrease with increasing ℓ/h ratio.

Intuitively, it is reasonable to expect such a point to occur if one considers that a grouser plate consists of two elements; a flat plate sliding on the soil surface, and a vertical blade. At low values of h, and hence at large values of shape factor, the flat plate mechanism will prevail and the resulting horizontal forces will be described by a straight line at some small negative slope. Correspondingly, at larger values of h (i.e., small values of shape factor), the vertical blade mechanism will govern grouser behaviour and the horizontal force - shape factor relationship will be given by a straight line inclined at a large negative slope to the abscissal axis. Since the actual grouser behaviour is a combination of these two modes, a "singularity" will occur at the point of intersection of the two lines.

Numerical calculations were attempted as a means of justifying the above considerations. However, several difficulties are associated with these calculations. The ratio ℓ/h, while being allowed to vary, was calculated with the value of ℓ kept constant at 3 inches. Consequently, in order for ℓ/h to approach zero, the value of h must become very large.

In an attempt to overcome this problem, the ratio was allowed to go to zero by numerically setting ℓ equal to zero and selecting h equal to 3 inches. Assuming passive pressure conditions, the horizontal force exerted by the soil on the vertical grouser face was then computed and found to be equal to 94.5 pounds. An examination of Figure 4-7 will show that the intercept of the curve and the ordinate axis will occur at some value in excess of 94.5 pounds which is consistent with the idea that for ℓ/h to go to zero, in this case, the value of h will have to be very large.

Finally, the variation of measured vertical force with shape factor is shown in Figure 4-8. It will be readily seen that the general shape of the curve is similar to that shown in Figure 4-6, expressing the variation of horizontal force with grouser geometry.

From the foregoing considerations, it would appear that an optimum value of shape factor exists which, in this case, was in the region of 1.7. No estimate can be made as to whether this value is peculiar to

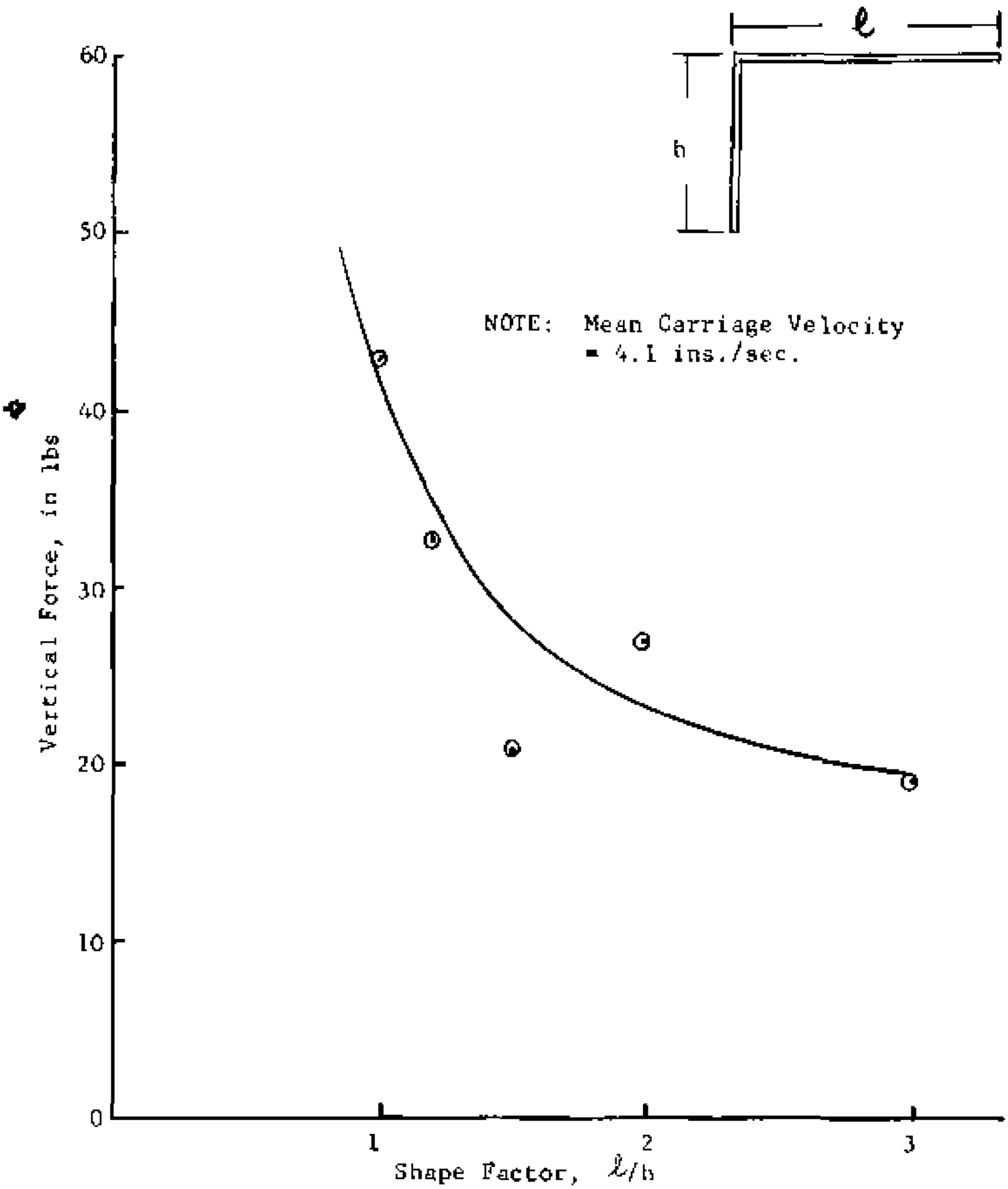

FIGURE 4-8. INFLUENCE OF GROUSER GEOMETRY ON MEASURED VERTICAL FORCES FOR CONSTANT ELEVATION TESTS

the present test conditions and further research needs to be carried out to determine the significance of this point.

4.7 VARIATION OF ANGLE OF INCLINATION, β, WITH SYSTEM AND GROUSER PARAMETERS

The variations of β with carriage velocity, shape factor and applied vertical load have been shown in Figures 3.3 and 3.4. The variation of β with applied vertical load is shown in Figure 4-9 and the results are consistent with the variation of the horizontal forces with applied vertical load (Figure 4-2). It will be seen that the horizontal force increases slowly with an increase in vertical load up to a load level of about 32 pounds. At values of load in excess of this, the slope of the curve shown in Figure 4-2 begins to increase. This is consistent with the increase in β exhibited at load levels less than 32 pounds. At this point, the value of β becomes a maximum and then begins to decrease; the decrease corresponding to an increase in stress function and hence, in horizontal force (Figure 4-9). Consequently, for values of applied vertical load less than 32 pounds, the magnitude of the increase in the force component resulting from the increase in vertical load tends to be reduced by the decrease in the force component contributed by the radial shear and Rankine zones. At vertical loads in excess of 32 pounds, the opposite holds true and the force components reinforce each other.

In addition, a summary of the changes in β with speed and shape factor is shown in Figure 4-9 for a constant vertical load of 21-1/2 pounds. It is apparent that the general tendency is for β to decrease with increasing grouser depth while β tends to increase for increasing

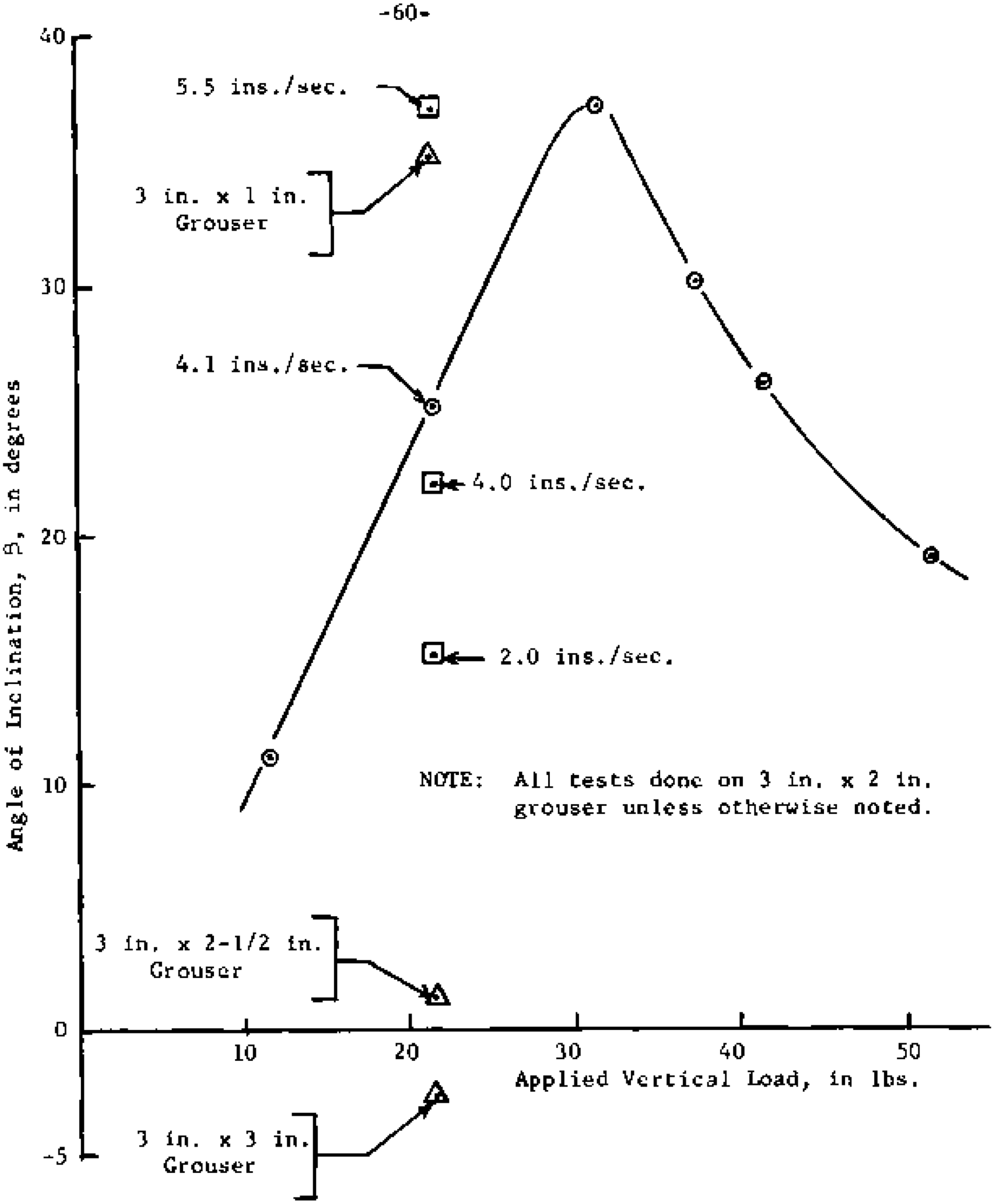

(Mean Carriage Velocity = 4.1 ins./sec. unless otherwise specified)

FIGURE 4-9. VARIATION OF β WITH APPLIED VERTICAL LOAD velocity. As such, any optimum design of a grouser for variable speed conditions at a given value of applied vertical load must take these effects into consideration.

4.8 COMPARISON OF CONSTANT ELEVATION AND CONSTANT VERTICAL LOAD TESTS

It will be apparent on comparing analogous results for the constant elevation and constant vertical load tests that the former exhibit higher values of horizontal force. This is consistent with the results shown in Table A-1. It will be observed in this table, that the sum of the measured vertical forces and the restraining force, which was at all times equal to 12 pounds for the constant elevation tests, is consistently greater than the applied vertical load in the constant vertical load tests. In addition, it will be noted in Figure 3-3 that the variation of β with carriage velocity for the constant elevation tests is shown as a broken line and ignores one point at a carriage velocity of 5 inches per second and at an angle of inclination of -5°. This point is not representative of the general trend of variation in β and since no reason could be found for the shape of the curve which would result from an inclusion of this point, it was neglected. It must be emphasized however, that the broken line only represents a suggested variation in this case.

Finally, the plots of horizontal and vertical components of particle velocity, relative to the carriage velocity, are shown in Figures 4-10 and 4-11 respectively. These results are typical of the iso-velocity contours in all tests and serve to show that the assumption of zone O'ABO as being rigid is a justifiable one. This will be readily seen from the fact that the relative velocities in this zone are zero.

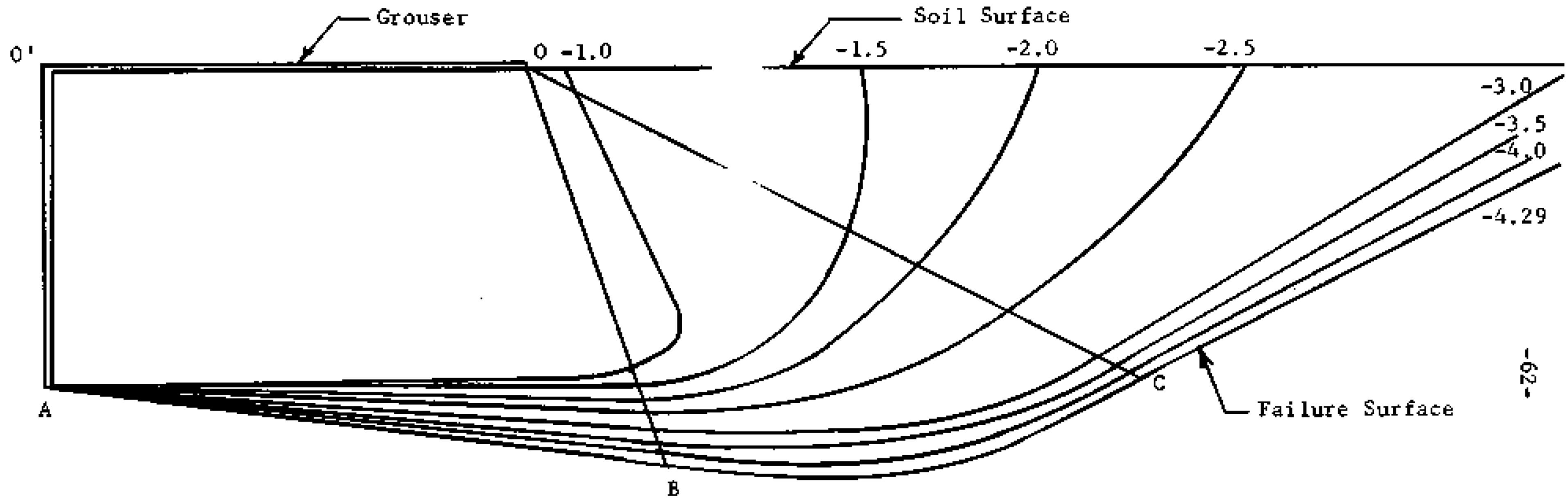

(Carriage Velocity = 4.29 ins./sec.; ϕ = 38°; β = 19°; grouser 3 ins. x 2 ins.)

FIGURE 4-10. LINES OF EQUAL HORIZONTAL COMPONENT OF PARTICLE VELOCITY, v_x INS./SEC., RELATIVE TO GROUSER VELOCITY, FOR TEST NO. 16

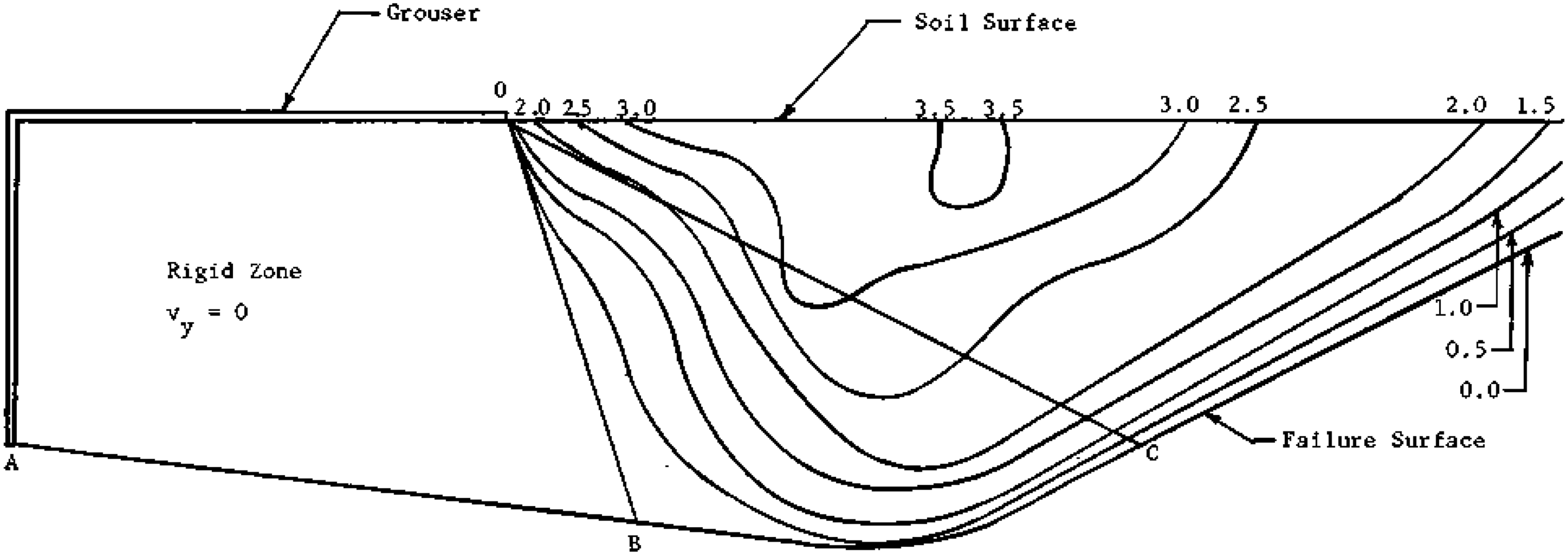

(Carriage Velocity = 4.29 ins./sec.; $\phi = 38^{\circ}$, $\beta = 19^{\circ}$, Grouser 3 ins. x 2 ins.)

FIGURE 4-11. LINES OF EQUAL VERTICAL COMPONENT OF PARTICLE VELOCITY, v_y, IN INS./SEC. RELATIVE TO CARRIAGE VELOCITY FOR TEST NO. 16

CHAPTER 5

APPLICATIONS AND CONCLUDING REMARKS

5.1 APPLICATION AND REMARKS

Since the aim of any general study on grouser-soil interaction is to achieve a better rationale for the design of grousers and the spacing of such grousers on a track, it becomes necessary to understand the mechanics of grouser-soil interaction.

For a $c = 0$ material (sand), it has been shown from this study that a means exists whereby one can predict grouser performance in terms of developed horizontal force under the aggressive action of the grouser (see Figures 4-1 and 4-2). The problem of system parametric variations can be accounted for and resolved in the theoretical computations to provide for a reasonable accuracy in predicting values for the developed horizontal force.

Specifically, the procedure to predict general grouser performance in sand entails:

1. Determine the α and β (see Figure 2-2) parameters experimentally. Alternatively, a set of α, β curves can be generated from this study; for example a list of values such as those in Table A-2 in the Appendix may be obtained.

2. With the procedure developed in Chapter 3 and the curves for S and ψ' as functions of θ, the developed forces under aggressive grouser action may be computed. It is understood that the failed mass under a single grouser may be estimated (or computed) using computations arising from the use of the method of characteristics.

Whilst the use of the limit equilibrium approach constrains the system to act in a certain ideal manner, it has been shown that slight aberrations from ideal behaviour can be tolerated - as evidenced from the close agreement between theoretically computed and experimentally measured values. Thus, insofar as the physical model corresponds to the mathematical model, a fair degree of success can be achieved in predicting grouser performance.

It would appear from the results of the study and the approach, that when minimization of β occurs, a greater horizontal grouser force is developed. From this study, it appears that an ℓ/h ratio of about 1.7 provides for the greatest minimization of β, (and correspondingly the optimum value for the developed horizontal grouser force).

With regard to the spacing of grousers, the evidence shows that so long as the Rankine zone is allowed to form with no hindrance from adjacent grousers, maximum horizontal forces can be developed. Thus, as has been stated previously by others, succeeding grousers should be placed outside the Rankine zone of influence (see Fig. 2.2). In view of the variability of β and α, it would be advisable to seek a solution in terms of anticipated or "worst" values of α and β.

5.2 WHERE DO WE GO FROM HERE?

The success achieved in describing grouser-sand mechanics should provide a relatively sound basis for further study with other soil types. Specifically, since the $c=0$ case is well established, it now remains to seek a solution for the other extreme (and relatively common) case of a $\phi=0$ material - clays! Greater problems are anticipated in clays in view of the difficulties surrounding the condition of limit equilibrium throughout the entire failable zone. It would appear that perhaps some form of plasticity solution similar to that established by Yong and Webb (1969) would have to be developed. Much also remains to be done for mixed soils, i.e., $c \neq 0$, $\phi \neq 0$.

For general application of the present results, it would be most appropriate, at this time to determine whether the α and β values determined may be applied to other systems (i.e., experimental and field). Theory suggests that if the constraints in this present study have been properly controlled, the α and β values given in Table A-2 and Figures 3-3 and 3-4 should be generally applicable. In addition, it would be generally desirable to test the validity of the grouser geometrical ratio of about 1.7 for suitability in optimization of developed aggressive force from the grouser.

Field application of general theory would be appropriate at this time. It is imagined that a new set of constraints would be necessarily imposed.

BIBLIOGRAPHY

Bekker, M.G. (1956), "The Theory of Land Locomotion", University of Michigan Press, Ann Arbor, Michigan.

Bekker, M.G. (1960), "Off the Road Locomotion", University of Michigan Press, Ann Arbor, Michigan.

Chen, C.K. (1969), "Experimental and Theoretical Study of Soil Cutting", M.Eng. Thesis, McGill University, Montreal.

Cox, A.D., Eason, G. and Hopkins, H.G. (1961), "Axially Symmetric Plastic Deformation in Soils", Philosophical Trans. Royal Soc. of London, Series A, Vol. 254, p. 1.

Drucker, D.C. and Prager, W. (1952), "Soil Mechanics and Plastic Analysis or Limit Design", Quarterly of Applied Mathematics, Vol. 10, p. 157.

Drucker, D.C. (1961), "On Stress-Strain Relations for Soils and Load Carrying Capacity", Proc. 1st Int. Conf. on the Mech. of Soil-Vehicle Systems, Turin, p. 15.

Freitag, D.R. (1965), "Wheels on Soft Soils; An Analysis of Existing Data", Tech. Report No. 3-670, U.S. Army Eng. Wat. Expt. Sta., Vicksburg, Mississippi.

Guskov, V.V. (1968), "Effect of Forward Speed on the Drawbar Performance of a Track-Laying Tractor", J. Agric. Engr. Res., Vol. 13, No. 3, p. 203.

Harr, M.E. (1966), "Foundations of Theoretical Soil Mechanics", McGraw-Hill Book Co., New York.

Haythornthwaite, R.M. (1961), "Methods of Plasticity in Land Locomotion Studies", Proc. 1st Int. Conf. on the Mech. of Soil-Vehicle Systems, Turin, p. 28.

Janozi, Z. and Hanomoto, B. (1961), "The Analytical Determination of Drawbar Pull as a Function of Slip for Tracked Vehicles in Deformable Soils", Proc. 1st Int. Conf. on the Mech. of Soil-Vehicle Systems, Turin, p. 707.

Japp, R.D. (1964), "Considerations in the Dynamics of Clay Soils", M.Eng. Thesis, McGill University, Montreal.

Kirkpatrick, W.M. (1957), "Condition of Failure for Sands", Proc. 4th. Int. Conf. of Soil Mechanics and Foundation Engineering, Vol. 1, p. 167.

McKyes, E. (1969), "Yielding of a Remoulded Clay Under Complex Stress States", Ph.D. Thesis, McGill University, Montreal.

Micklethwait, E.W.E. (1944), "Soil Mechanics in Relation to Fighting Vehicles", Military College of Science, Chertsey, England.

Prager, W. (1953), "A Geometrical Discussion of the Slip Line Field in Plane Plastic Flow", Trans. Royal Inst. Tech., Stockholm, Sweden, Nr. 65, p. 1.

Reece, A.R. (1965), "Principles of Soil-Vehicle Mechanics", Proc. Inst. Mech. Engrg. (Automobile Div.), Vol. 180, Part 2A, p. 1.

Savage, S.B. (1965), "The Mass Flow of Granular Materials Derived From Coupled Velocity Stress Fields", British J. Appl. Phys., Vol. 16, p. 1885.

Seia, A.D. (1961), "On the Slip and Tractive Effort", Proc. 1st Int. Conf. on the Mech. of Soil-Vehicle Systems, Turin, p. 587.

Shield, R.T. (1953), "Mixed Boundary Valve Problems in Soil Mechanics", Quart. Appl. Math., Vol. 11, p. 61.

Shih, C.F. (1968), "Static Analysis of Soil-Grouser Interaction Process", Unpublished Report, McGill University, Montreal.

Sokolovski, V.V. (1960), "Statics of Soil Media", Butterworth's Scientific Publications, London, 2nd Edition.

Spencer, A.J.M. (1964), "A Theory of the Kinematics of Ideal Soils Under Plane Strain Conditions", J. Mech. Phys. Solids, Vol. 12, p.337.

Takagi, S. (1962), "Plane Plastic Deformation of Soils", J. Eng. Mech. Div., Proc. ASCE, Vol. 88, EM 3, p. 107.

Terzaghi, K. (1944), "Theoretical Soil Mechanics", John Wiley and Sons, New York.

Trafficability Research Team (1961), "A Suggested Empirical Combination Between the Bekker and the Vicksburg Methods in Trafficability Analyses of Deep Loose Sands", Proc. 1st Int. Conf. on the Mech. of Soil-Vehicle Systems, Turin, p. 837.

Wills, B.M.D., Barret, F.M. and Shaw, G.J. (1965), "An Investigation into Rolling Resistance Theories for Towed Rigid Wheels", J. Terramechanics, Vol. 2, No. 1.

Yong, R.N., Boyd, C.W. and Webb, G.L. (1967), "Experimental Study of Behaviour of Sand Under Moving Rigid Wheels", McGill University, Soil Mechanics Series, No. 20.

Yong, R.N., Chen, C.K. and Sullivan, R.J. (1969), "Application of Limit Analysis to Soil Cutting", Paper for 3rd Int. Conf., ISTVS, Essen, West Germany.

Yong, R.N. and Osler, J.C. (1966), "On the Analysis of Soil Deformation Under a Moving Rigid Wheel", Proc. 2nd Int. Conf., ISTVS, Quebec, p. 339.

Yong, R.N. and Webb, G.L. (1969), "Energy Dissipation and Drawbar Pull Prediction in Soil-Wheel Interaction", Paper for 3rd Int. Conf., ISTVS, Essen, West Germany.

Yong, R.N., Fitzpatrick-Nash, J.D. and Webb, G.L. (1968), "Response Behaviour of Soil Under a Moving Rigid Wheel", Report DRTE (Geophysics) 30, Soil Mechanics Series, No. 23, McGill University, Montreal.

APPENDIX

TABLE A-1

EXPERIMENTAL RESULTS

Test No.	Type of Test	Grouser Size (in.x in.)	Density (p.c.f)	Speed (in./sec.)	Applied Vertical Load (lb)	Horizontal Force H (lb)	Vertical Force V (lb)
7	C.V.L	3 x 2	98.38	5.32	21-1/2	21.27	
8	C.V.L	3 x 2	98.73	5.91	21-1/2	25.38	
9	C.V.L	3 x 2	100.93	5.25	21-1/2	22.30	
10	C.V.L	3 x 2	100.93	1.59	21-1/2	34.50	
11	C.V.L	3 x 2	100.25	1.64	21-1/2	19.30	
12	C.V.L	3 x 2	101.17	1.61	8-1/2	6.09	
13	C.V.L	3 x 2	100.48	3.94	11-1/2	18.20	
14	C.V.L	3 x 2	102.20	3.94	31-1/2	28.40	
15	C.V.L	3 x 2	99.87	4.10	37-1/2	30.30	
16	C.V.L	3 x 2	101.60	4.05	51-1/2	53.40	
17	C.V.L	3 x 2	100.79	4.29	21-1/2	21.30	
18	C.V.L	3 x 2	99.75	4.00	21-1/2	18.30	
19	C.E	3 x 2	100.25	3.82		35.50	22.50
20	C.E	3 x 2	100.42	4.00		38.00	20.30
21	C.E	3 x 2	100.73	1.23		30.40	13.50
22	C.E	3 x 2	99.72	4.09		35.50	
23	C.E	3 x 2	97.99	5.32		43.00	21.20
24	C.E	3 x 2	100.90	5.32		50.70	32.40
27	C.E	3 x 2	100.80	5.00		45.60	26.00
28	C.E	3 x 1	99.94	3.82		31.90	19.00
29	C.V.L	3 x 1	101.41	3.81	21-1/2	15.50	
30	C.V.L	3 x 1-1/2	100.34	3.83	21-1/2	24.10	
31	C.E	3 x 1-1/2	98.83	3.83		38.80	27.10
32	C.E	3 x 2-1/2	99.10	3.72		52.00	32.80
33	C.V.L	3 x 2-1/2	100.67	3.72	21-1/2	41.90	
34	C.V.L	3 x 3	100.60	3.72	21-1/2	50.50	
35	C.E	3 x 3	100.33	3.72		80.50	43.00

NOTE: Grouser size designated as $\ell \times h$.

C.V.L = constant vertical load test.

C.E = constant elevation test.

TABLE A-2

COMPUTER VALUES OF S_B, S_C, ψ'_B AND ψ'_C FOR $\phi = 38^\circ$, $\delta = 29.5^\circ$

Test No.	β°	S_B	S_C (Calculated)	S_C (Rankine)	S_C % Error	ψ'_B	$\psi'_C{}^\circ$ (Calculated)	$\psi'_C{}^\circ$ (Rankine)	$\psi'_C{}^\circ$ % Error	α°
8	27.0	3.450	1.1460	1.1406	0.49	48.693	25.493	26	2.0	-1.5
9	38.0	2.200	1.1387	1.1406	0.17	48.693	25.256	26	2.8	-2.5
11	14.5	5.400	1.1464	1.1406	0.52	48.693	25.369	26	2.4	-0.5
13	11.0	6.200	1.1392	1.1406	0.12	48.693	25.317	26	2.6	-3.5
14	37.0	2.300	1.1493	1.1406	0.11	48.693	25.574	26	1.6	0.5
16	19.0	4.650	1.1365	1.1406	0.36	48.693	25.238	26	2.9	7.5
17	25.0	3.725	1.1449	1.1406	0.38	48.693	25.345	26	2.5	-1.0
20	26.0	3.480	1.1401	1.1406	0.04	48.693	25.382	26	2.4	0.0
24	25.0	3.725	1.1455	1.1406	0.43	48.693	25.479	26	2.0	0.0
27	- 5.0	10.900	1.1364	1.1406	0.37	48.693	25.257	26	2.8	0.0
28	16.5	5.000	1.1503	1.1406	0.09	48.693	25.479	26	2.0	0.0
29	35.0	2.500	1.1419	1.1406	0.11	48.693	25.363	26	2.5	1.0
30	32.5	2.760	1.1420	1.1406	0.12	48.693	25.410	26	2.1	-0.5
32	11.0	6.200	1.1392	1.1406	0.12	48.693	25.317	26	2.6	0.0
34	- 5.0	11.000	1.1437	1.1406	0.23	48.693	25.437	26	2.2	-1.0
35	- 2.5	9.900	1.1334	1.1406	0.63	48.693	25.084	26	3.5	0.0

NOTE: Positive values of α denote angles below horizontal.